Chapter 8

Inverse Problem of Leaf Area Estimation

Yang et al.

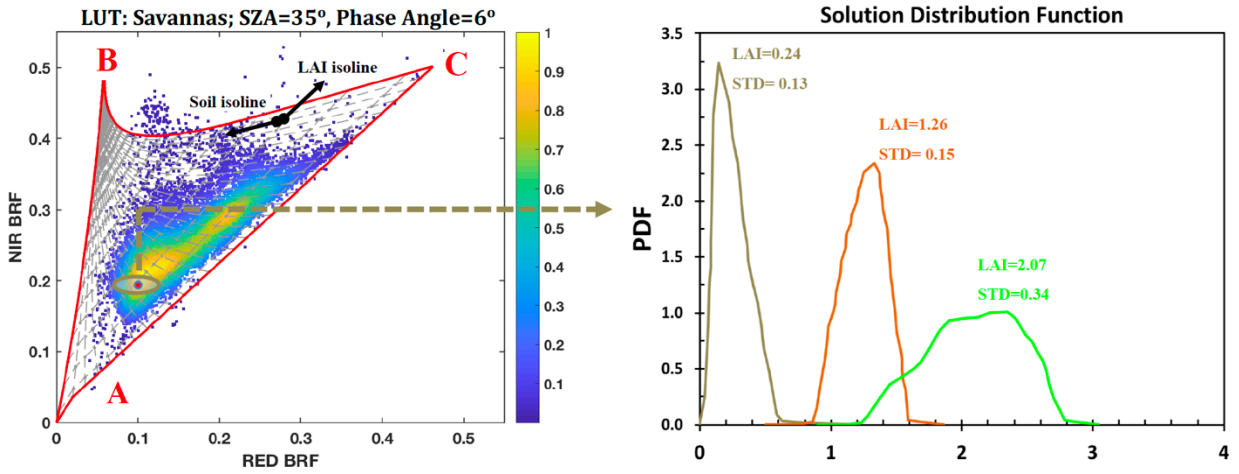

Remote Sensing of Environment 198 (2017) 69–84

Contents lists available at ScienceDirect

Remote Sensing of Environment

journal homepage: www.elsevier.com/locate/rse

Estimation of leaf area index and its sunlit portion from DSCOVR EPIC data: Theoretical basis

Bin Yang [a,b], Yuri Knyazikhin [a,*], Matti Mõttus [c], Miina Rautiainen [d,e], Pauline Stenberg [f], Lei Yan [b], Chi Chen [a], Kai Yan [a,g], Sungho Choi [a], Taejin Park [a], Ranga B. Myneni [a]

[a] Department of Earth and Environment, Boston University, Boston, MA 02215, USA
[b] Beijing Key Laboratory of Spatial Information Integration and 3S Application, School of Earth and Space Sciences, Peking University, Beijing 100871, China
[c] VTT Technical Research Centre of Finland, PO Box 1000, FI-02044 VTT, Finland
[d] Aalto University, School of Engineering, Department of Built Environment, P.O. Box 14100, FI-00076 Aalto, Finland
[e] Aalto University, School of Electrical Engineering, Department of Electronics and Nanoengineering, P.O. Box 13000, FI-00076 Aalto, Finland
[f] Department of Forest Sciences, University of Helsinki, P.O. Box 27, FI-00014, Finland
[g] School of Geography, Beijing Normal University, Beijing 100875, China

ARTICLE INFO

Article history:
Received 16 August 2016
Received in revised form 11 May 2017
Accepted 24 May 2017
Available online xxxx

Keywords:
DSCOVR mission
Sunlit leaf area index
Spectral invariants
Hot spot
Operational algorithm
Radiative transfer

ABSTRACT

This paper presents the theoretical basis of the algorithm designed for the generation of leaf area index and diurnal course of its sunlit portion from NASA's Earth Polychromatic Imaging Camera (EPIC) onboard NOAA's Deep Space Climate Observatory (DSCOVR). The Look-up-Table (LUT) approach implemented in the MODIS operational LAI/FPAR algorithm is adopted. The LUT, which is the heart of the approach, has been significantly modified. First, its parameterization incorporates the canopy hot spot phenomenon and recent advances in the theory of canopy spectral invariants. This allows more accurate decoupling of the structural and radiometric components of the measured Bidirectional Reflectance Factor (BRF), improves scaling properties of the LUT and consequently simplifies adjustments of the algorithm for data spatial resolution and spectral band compositions. Second, the stochastic radiative transfer equations are used to generate the LUT for all biome types. The equations naturally account for radiative effects of the three-dimensional canopy structure on the BRF and allow for an accurate discrimination between sunlit and shaded leaf areas. Third, the LUT entries are measurable, i.e., they can be independently derived from both below canopy measurements of the transmitted and above canopy measurements of reflected radiation fields. This feature makes possible direct validation of the LUT, facilitates identification of its deficiencies and development of refinements. Analyses of field data on canopy structure and leaf optics collected at 18 sites in the Hyytiälä forest in southern boreal zone in Finland and hyperspectral images acquired by the EO-1 Hyperion sensor support the theoretical basis.

1. Introduction

The NASA's Earth Polychromatic Imaging Camera (EPIC) onboard NOAA's Deep Space Climate Observatory (DSCOVR) mission was launched on February 11, 2015 to the Sun-Earth Lagrangian L1 point where it began to collect radiance data of the entire sunlit Earth every 65 to 110 min in June 2015. It provides imageries in near backscattering directions with the scattering angle between 168° and 176° at ten ultraviolet to near infrared (NIR) narrow spectral bands centered at 317.5 (band width 1.0) nm, 325.0 (2.0) nm, 340.0 (3.0) nm, 388.0 (3.0) nm, 433.0 (3.0) nm, 551.0 (3.0) nm, 680.0 (3.0) nm, 687.8 (0.8) nm, 764.0 (1.0) nm and 779.5 (2.0) nm (https://epic.gsfc.nasa.gov/epic). The reflectance of vegetation reaches its maximum in the backscattering direction. This phenomenon is known as the hot spot effect (Gerstl, 1999 Knyazikhin and Marshak, 1991 Kuusk, 1991 Qin et al., 1996 Ross and Marshak, 1988). It has been widely recognized that the hot spot region represents the most information-rich directions in the directional distribution of canopy reflected radiation (Gerstl, 1999 Goel et al., 1997 Qin et al., 2002 Ross and Marshak, 1988). The uniqueness of the DSCOVR EPIC observing strategy is its ability to provide frequent observations of every region of the Earth in near hot spot directions that the existing Low-Earth-Orbiting and Geostationary satellites do not have. The EPIC level 1 data and accompanying documentation are available from the NASA Langley Atmospheric Science Data Center (https://eosweb.larc.nasa.gov/project/dscovr/dscovr_table).

The EPIC team is responsible for development and validation of algorithms for producing a series of products which include vegetation green Leaf Area Index (LAI) and its sunlit portion at 10 km spatial

* Corresponding author at: Earth and Environment, Boston University, 675 Commonwealth Avenue, Boston, MA 02215, USA.
E-mail address: jknjazi@bu.edu (Y. Knyazikhin).

http://dx.doi.org/10.1016/j.rse.2017.05.033
0034-4257/

resolution. Whereas LAI is a standard product of many satellite missions (Garrigues et al., 2008 Yan et al., 2016b), the Sunlit Leaf Area Index (SLAI) is a new satellite-derived parameter. Sunlit and shaded leaves exhibit different radiative response to incident Photosynthetically Active Radiation (400–700 nm) (Mercado et al., 2009 Stenberg, 1998), which in turn triggers various physiological and physical processes required for the functioning of plants. Leaf area and its sunlit portion are key state parameters in most ecosystem productivity models (Bonan et al., 2003 Chen et al., 2012 Dai et al., 2004 He et al., 2013 Mercado et al., 2009 Norman, 1982) and carbon/nitrogen cycle (Chen et al., 2003 Doughty and Goulden, 2008 Wang et al., 2001). Our objective is to develop an algorithm for the retrieval of leaf area index and diurnal course of sunlit leaf area index from EPIC Bidirectional Reflectance Factor (BRF) of vegetated land.

LAI and SLAI are defined as the total hemi-surface (Chen and Black, 1992) and sunlit leaf areas per unit ground area. We adapt the retrieval approach implemented in the MODIS operational LAI/FPAR algorithm to retrieve these parameters (Knyazikhin et al., 1998a Knyazikhin et al., 1998b). The algorithm compares measured spectral BRF with those evaluated from model-based entries stored in a look-up-table (LUT). All canopy structural variables and ground reflectance for which modeled and measured BRFs agree within uncertainties in the observed and modeled canopy reflectances are considered as acceptable solutions. The mean value of a structural variable of interest (LAI, SLAI) and its dispersion are taken as the solution of the inverse problem and its retrieval uncertainty. In addition to the measured BRFs, the observation and model uncertainties are also inputs to the retrieval technique (Wang et al., 2001). The former come largely from the correction of the in-orbit data for atmospheric and other environmental effects whereas the latter are determined by the range of natural variation in biophysical parameters not accounted for by the LUT.

A biome classification map is another important ancillary data layer used as input to the algorithm. The global classification of canopy structural types utilized in the Collection 6 MODIS LAI/FPAR algorithm is adopted (Yan et al., 2016a). Global vegetation is stratified into eight canopy architectural types, or biomes. The eight biomes are grasses and cereal crops, shrubs, broadleaf crops, savannas, evergreen broadleaf forests, deciduous broadleaf forests, evergreen needle leaf forests and deciduous needle leaf forests. The biome map reduces the number of unknowns in the inverse technique through the use of simplifying assumptions. The LUT is generated for each biome type. The 8-biome map is provided by the MODIS Global Land Cover Type product (https://lpdaac.usgs.gov/dataset_discovery/modis/modis_products_table).

Thus, the EPIC algorithm inputs BRFs at red (680.0 nm) and NIR (779.5 nm) spectral bands, their uncertainties, canopy structural type, and outputs mean LAI, SLAI and their dispersions. The LUT is a key element of the retrieval technique that determines its performance. Our primary objective is to develop a new LUT that incorporates recent advances in the theory of canopy spectral invariants, accounts for the uniqueness of the EPIC observation geometry and allows for the integration of retrieving SLAI into the operational MODIS LAI algorithm. Our goal is not only to incorporate spectral invariants into the retrieval technique but also resolve known issues in the theory. The hot spot phenomenon is one of them. A special emphasis therefore is given to its integration into the spectral invariant technique.

Whereas protocols for validation of satellite derived LAI are well advanced (Garrigues et al., 2008), there are neither ground truth SLAI data nor methods for obtaining such data from field measurements. Our secondary objective therefore is to outline approaches to ground measurements that would allow us not only to validate satellite derived SLAI but also help product developers to identify deficiencies in the operational algorithm and develop refinements.

This paper is organized as follows. A parameterization of the process of photon-canopy interactions in terms of spectrally invariant parameters and how they are linked to variables measurable in the field are discussed in Section 2 and Appendices A–C. Study area, field data on canopy structure, leaf and ground spectral reflectance as well as hyperspectral images needed to validate the LUT are described in Section 3. The stochastic radiative transfer equations are used to generate the LUT entries. Its initialization and analyses of its ability to provide relationships between BRF and canopy structural variables are demonstrated in Sections 4, 5 and Appendix D. The differences between the MODIS and EPIC LUTs are discussed in Section 6. Finally, Section 7 summarizes the results.

2. Theoretical basis

We introduce a directional variable, Visible Fraction of Leaf Area, VFLA(Ω) defined as the fraction of the total hemi-surface leaf area that is visible from outside the canopy along the direction $-\Omega$. Visible Leaf Area Index, VLAI(Ω), in the direction Ω is the product of LAI and VFLA. Their values give the Sunlit Fraction of Leaf Area (SFLA) and Sunlit Leaf Area Index (SLAI) in the hot spot direction, i.e., when the direction Ω coincides with the direction to the sun. Understanding the relationship between canopy BRF, VFLA and VLAI is our main focus.

The fraction of photons incident on the canopy that are intercepted by phytoelemets is called the canopy interceptance (Stenberg et al., 2016). The canopy directional uncollided transmittance is the fraction of photons that are transmitted directly through gaps in the canopy. These variables depend on canopy structure and vary with the solar direction. We use the symbols $i_0(\Omega)$ and $t_0(\Omega)$ to signify the interceptance of, and directional uncollided transmittance through, the vegetation illuminated from above by a monodirectional beam in the direction $-\Omega$. Clearly, $i_0(\Omega)+t_0(\Omega)=1$. Note that $t_0(\Omega)$ can be estimated from field measurements of canopy transmitted radiation using, e.g., a directional gap fraction sensor LAI-2000 PCA (Rautiainen and Stenberg, 2015). The VFLA(Ω), $i_0(\Omega)$ and $t_0(\Omega)$ do not depend on wavelength.

The intercepted photons initiate the process of photon-canopy multiple interactions. We will use the concept of recollision probability to describe this process (Huang et al., 2007 Knyazikhin et al., 2011 Stenberg, 2007 Stenberg et al., 2016 Wang et al., 2003). This variable is the probability that a photon scattered by a phytoelement in the canopy will interact within the canopy again. The scattered photons can escape the vegetation through gaps between phytoelements. This event is quantified by the escape probability. Fig. 1 illustrates these definitions. The solid arrows depict photons incident on both sides of leaf surfaces from different directions. Their total number is N. A fraction of these photons will be scattered and hit leaves again (dashed arrows). The

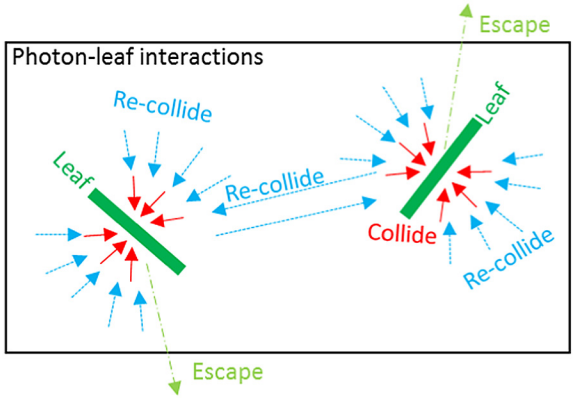

Fig. 1. Recollision and escape probabilities. Solid arrows depict photons incident on leaf surfaces from different directions. A fraction of these photons will be scattered and hit leaves again (dashed arrows). The scattering event is quantified by the wavelength dependent leaf albedo, ω_λ, defined as the fraction of radiation incident on a leaf that is reflected or transmitted. Given total numbers, N and N', of photons incident on leaf surfaces before ("solid arrows") and after one interaction ("dashed arrows") with leaves, the recollision probability is just $p=N'/(\omega N)$. The directional escape probability is the probability by which a scattered photon will escape the vegetation in a given direction Ω ("dash-dot arrows").

scattering event is quantified by the wavelength dependent leaf albedo, ω_λ, defined as the fraction of radiation incident on the leaf that is reflected, or transmitted. Let N' be the total number of scattered photons that hit leaves ("dashed arrows" in Fig. 1). Given N, N' and ω_λ, the recollision probability is $p = N'/(\omega_\lambda N)$. With the probability $(1-p)$ the scattered photons will escape the vegetation. Their angular distribution is given by the directional escape probability density, $\rho(\Omega)$, defined as $\rho(\Omega)|\mu|\,d\Omega = \pi M(\Omega)d\Omega/(\omega_\lambda N)$. Here $M(\Omega)d\Omega$ is the number of scattered photons exiting the canopy in the direction Ω ("dash-dot arrows"); $\mu = \cos\theta$ and θ is the polar angle of Ω. Spherical integration of $\pi^{-1}\rho(\Omega)|\mu|$ results in $(1-p)$. Note that whereas the leaf albedo depends on wavelength, the recollision and escape probabilities are determined by the structure of the canopy rather than photon frequency or the optics of the canopy (Knyazikhin et al., 2011). Our goal is to parameterize the process of photon-canopy interactions in terms of spectrally invariant parameters that include VFLA, canopy interceptance, recollision and escape probabilities.

2.1. A simple canopy radiative regime, VFLA and spectral invariants

It follows from the above definitions that the recollision and escape probabilities depend on radiation field in the vegetation canopy, i.e., on the magnitude and angular distribution of radiation incident on leaf surfaces. We start our analyses with the simplest case where non-absorbing leaves ($\omega_\lambda = 1$) in a vegetation canopy are illuminated by spatially independent isotropic radiation. Here we use a simple stochastic model of canopy structure to evaluate the spectrally invariant parameters. In this model the vegetation canopy is treated as a stationary Poisson germ-grain stochastic process (Fig. 2 and Appendix A). For each realization of the canopy structure we count (a) scattered photons that recollide or (b) exit the canopy in a given direction Ω, and (c) leaf area (number of segments, Fig. 2b) from which scattered photons can exit the canopy through gaps along the direction Ω. From this statistics, canopy interceptance, $i_0(\Omega)$, visible fraction of leaf area, VFLA(Ω), recollision, p_{iso}, and directional escape, $\rho_{iso}(\Omega)$, probabilities are estimated (Appendix A). We use the subscript "*iso*" to designate the special case when leaves are subjected to isotropic radiation. In Sections 2.3–2.4 we will analyze this technique in the case of more realistic heterogeneous canopies under varying within-canopy radiation field.

In our simple model, the directional uncollided transmittance follows Beer's exponential transmission law, i.e., $t_0(\Omega) = \exp(-\tau(\Omega))$ where $\tau(\Omega) = G(\Omega)LAI/|\mu|$ represents the mean optical path in the direction Ω and $G(\Omega)$ is the geometry factor defined as the mean projection of unit leaf area onto a plane perpendicular to the direction Ω (Ross, 1981 Stenberg, 2006). The visible leaf area index can be estimated as $\mathrm{VLAI} = i_0(\Omega)|\mu|/G(\Omega)$ (Wilson, 1967). It follows from these relationships that the visible fraction of leaf area is the ratio between canopy interceptance and the mean optical path, which can be expressed in terms of the canopy directional uncollided transmittance as

$$\mathrm{VFLA}(\Omega) = \frac{1 - t_0(\Omega)}{|\ln(t_0(\Omega))|}. \quad (1)$$

Fig. 3a shows VFLA vs. LAI curve derived from the stochastic simulations of canopy structure can be accurately approximated by Eq. (1) in the case of spherically oriented leaves. Fig. 3b shows that this is true for other types of leaf orientation.

Eq. (1) is expressed in terms of the directional uncollided transmittance, a variable that can be estimated from field measurements of canopy transmitted radiation (Rautiainen and Stenberg, 2015). In real canopy the mean optical path depends on foliage clumping. For example, if we replace discs in the stochastic model with coniferous shoots the mean optical path becomes $\tau(\Omega) = G(\Omega)fLAI/|\mu|$. The clumping factor f converts area of needles on the shoot to the shoot silhouette area, which actually is the visible fraction of needle areas of the shoot. The VFLA calculated using Eq. (1) should be multiplied by the clumping factor, f, to obtain its true value. In the general case Eq. (1) therefore results in the effective VFLA, i.e., visible leaf area, VLAI, normalized by the effective leaf area, $f \cdot LAI$. The visible leaf area index is then $VLAI = VFLA \cdot f \cdot LAI$. It follows from this simple relationship that VLAI is independent of the clumping factor in the sense that its specification does not depend on whether true values, $(VFLA \cdot f)$ and LAI, or their effective counterparts, $VFLA$ and $(f \cdot LAI)$, are used. This property provides a simple approach to derive VLAI from field data. Indeed, both the effective VFLA and effective LAI can be estimated from measured directional uncollided transmittance. The former is calculated using Eq. (1) whereas the latter using the standard technique based on Miller (1967) equation.

In our simple model, the directional escape probability density is related to canopy interceptance as

$$\rho_{iso}(\Omega) = 0.5\frac{i_0(\Omega)}{LAI}. \quad (2)$$

Spherical integration of $\pi^{-1}\rho_{iso}(\Omega)|\mu|$ results in the following relationships

$$\frac{1}{\pi}\int_{4\pi} \rho_{iso}(\Omega)|\mu|d\Omega = 1 - p_{iso} = \frac{i_{dif}}{\mathrm{LAI}}. \quad (3)$$

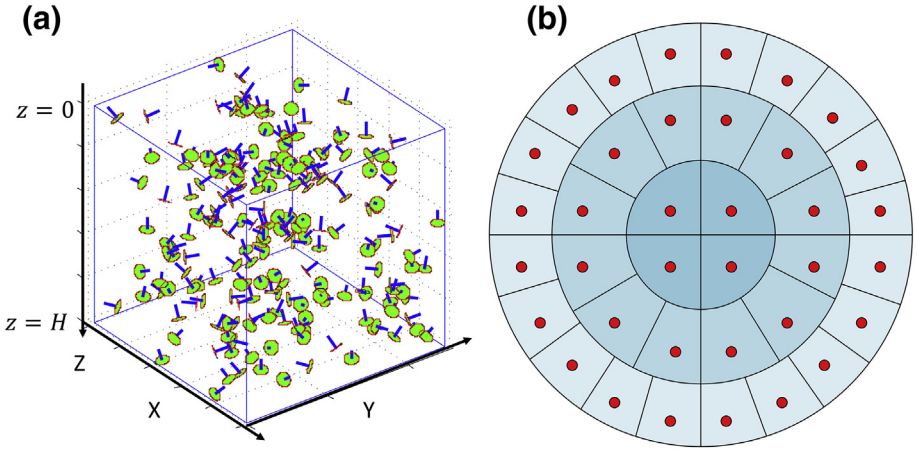

Fig. 2. Stochastic model of canopy structure. Points are scattered in a volume V according to a stationary Poisson point process of intensity d (panel a). On each of these points a disc of radius r (panel b) is placed. Their random orientation is generated with a leaf normal distribution function. The discs represent bi-Lambertian leaves, i.e., the incident photons are reflected from, or transmitted though, the disc in a cosine distribution about its upward normal. The disc is divided into n equal areas, which represent smallest resolvable scale. Panel (a) shows a realization of canopy structure with 207 leaves, each containing $n = 36$ equal areas. The leaf radius to canopy height ratio, r/H, and mean leaf area volume density, u_L, are 0.03 and 0.5, respectively. Leaf normals are shown as blue bars. More details are in Appendix A.

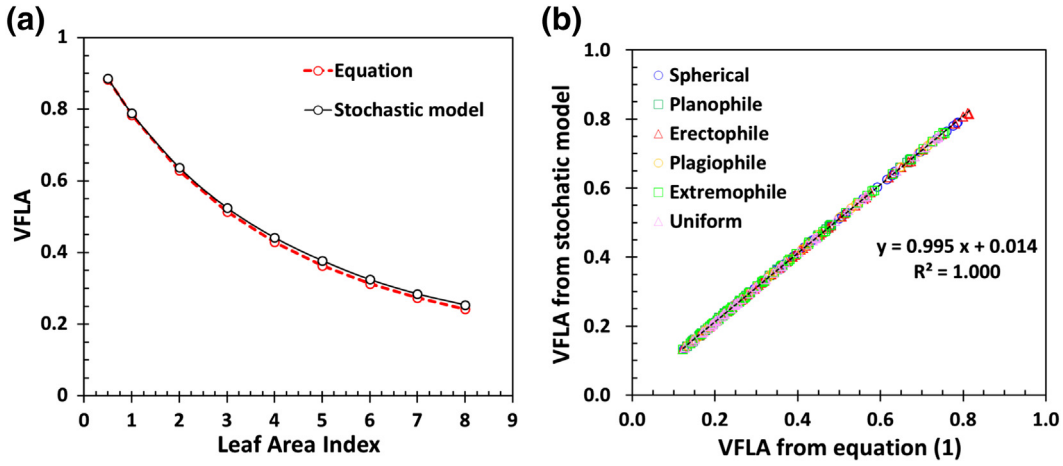

Fig. 3. Visible Fraction of Leaf Area (VFLA). Panel a: VFLA for spherically oriented leaves as a function of Leaf Area Index (LAI) for a zenith angle of 9.44° estimated directly from the stochastic model (legend "Stochastic model") and calculated with Eq. (1) (legend "Equation"). Panel b: Correlation between VFLA estimated from the stochastic model (vertical axis) and Eq. (1) (horizontal axis) for LAI and zenith angle ranges from 1 to 8, and from 0° to 60°, respectively. The scatter plot includes spherical, planophile, erectophile, plagiophile, extremophile and uniform leaves (Appendix A). The VFLAs from the stochastic model were estimated as described in Appendix A.

Here i_{dif} is the interceptance of the vegetation canopy illuminated by the isotropic sky radiation. This relationship was originally documented in Stenberg (2007). It follows from Eqs. (2) and (3) that

$$\frac{\rho_{iso}(\Omega)}{1-p_{iso}} = 0.5\frac{i_0(\Omega)}{i_{dif}}. \quad (4)$$

The left hand side of this equation is the fraction of photons exiting the canopy in the direction Ω relative to the total number of canopy leaving photons. Air- and satellite-borne sensors measure the canopy reflected radiation and thus the fraction of exiting photons can potentially be estimated from satellite data. On the other hand, it can also be derived from canopy directional uncollided transmittance. Eq. (4) therefore provides an important link between satellite and ground-based measurements.

Thus the VFLA, fraction of canopy leaving photons, recollision and escape probabilities for our simple model are expressed in terms of structural variables, $i_0(\Omega)$ and i_{dif}, which in turn can be estimated from below canopy measurements of the canopy directional uncollided transmittance using, e.g., the LAI-2000 plant analyzer (Rautiainen et al., 2009 Rautiainen and Stenberg, 2015 Stenberg, 2007). The VLAI and consequently SLAI can be estimated from VFLA without knowledge of foliage clumping and leaf normal orientation. Theoretically the VFLA could be derived from measurements of the above canopy radiation using Eqs. (1)–(4) if leaves were illuminated by a spatially homogeneous isotropic radiation. This of course is not the case in reality. The question then arises if there is a relationship between this simple case and real canopy reflectance. This will be discussed in Sections 2.3–2.4, which generalize the results to 3D heterogeneous canopy structure including clumping.

2.2. Stochastic reflecting boundary

The BRF of the vegetation reaches its maximum in the backscattering direction. This is so-called hot spot effect. The EPIC sensor therefore sees the brightest portion of the canopy reflected radiation. To account for the hot spot phenomenon in the spectral invariants we introduce a stochastic reflecting canopy boundary as points on leaf surfaces from which incident photons can enter the vegetation canopy. For a vegetation canopy illuminated by a monodirectional solar beam, the sunlit leaves form the boundary, which depends on the direction, $-\Omega_0$, of the incident beam and the distribution of sunlit leaves within the canopy space. Since the sunlit leaves can occur, with a certain probability, anywhere in the canopy, the boundary is subjected to both the direct solar beam and within-canopy diffuse radiation. The boundary scatters the intercepted photons, which in turn can exit or enter the canopy. The direct incident beam causes leaf shadowing. At strongly absorbing wavelength such as the blue or red spectral intervals a fraction of photons scattered by the boundary that enter the canopy will be absorbed with a high probability. This makes the diffuse radiation negligible. The canopy reflected radiation is mainly determined by the canopy boundary in this case. At weakly absorbing wavelength, e.g., the near infrared spectral region, the diffuse radiation is strong, which in turn tends to weaken the shadows and consequently makes the sunlit and shaded leaves less contrasting (Kuusk, 1991 Nilson, 1991).

The canopy boundary is an important structural parameter that impacts canopy reflective properties. To characterize its stochastic properties we use a Bi-directional Sunlit Fraction of Leaf Area, BSFLA(Ω&Ω_0), defined as a fraction of leaf area that is simultaneously visible from outside the canopy along directions, $-\Omega$ and $-\Omega_0$. Fig. 4a shows BSFLA for our simple stochastic model. We also plot VFLA(Ω), VFLA(Ω)VFLA(Ω_0) (Fig. 4a) and the correlation coefficient of VFLA(Ω) and VFLA(Ω_0) given by Eq. (A2) (Fig. 4b). There are two important features noteworthy in relation between the leaf areas. First, the events of seeing gaps from leaf surfaces in two directions are not independent (Fig. 4b and Eq. (A2) in Appendix A). This is effect of finite sizes of the foliage (Kuusk, 1991 Nilson, 1991), which in turn causes the canopy hot spot effect, i.e. a sharp increase in canopy reflected radiation when scattering direction Ω approaches the direction to the sun Ω_0 (Kuusk, 1991 Nilson, 1991 Qin et al., 1996 Ross and Marshak, 1988). Second, with the increase in the angle between Ω_0 and Ω, the correlation decreases from its maximum to zero, and then levels off (Fig. 4b). Its width decreases with a decrease of leaf sizes and vanishes for infinitesimal scatters. Beyond a point at which the correlation saturates, the events become uncorrelated.

The fraction of leaf surface areas "visible" outside the canopy along the direction $-\Omega$ can be expressed as VFLA(Ω) $=[1-h_{iso}(\Omega;\Omega_0)]$VFLA($\Omega$) $+h_{iso}(\Omega;\Omega_0)$VFLA($\Omega$). The summands represent fractions of shaded and sunlit leaf areas (Appendix A), and h_{iso} is the correlation coefficient of VFLA(Ω) and SFLA (Fig. 4b). The probability that photons scattered by shaded leaves will exit the vegetation in the direction Ω is $[1-h_{iso}(\Omega;\Omega_0)]\rho_{iso}(\Omega)$ (Appendix A). Some of the photons scattered by the boundary will escape vegetation canopy with unit probability. Their fraction is given by $j_{iso}(\Omega;\Omega_0)h(\Omega;\Omega_0)$ where j_{iso} is the anisotropy of the boundary reflected radiation, which is determined by the area scattering phase function and geometry factor (Appendix A).

Thus, the escape probability density, $\rho_{b,iso}(\Omega;\Omega_0)$, for our simple model with the stochastic boundary in the direction Ω_0 is a weighted

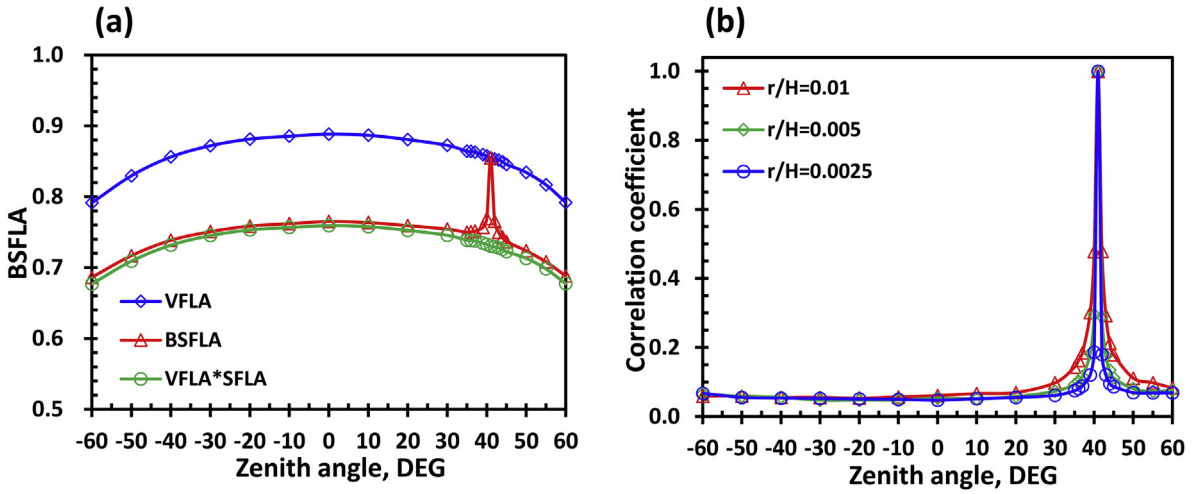

Fig. 4. Bi-directional Sunlit Fraction of Leaf Area, BSFLA($\Omega\&\Omega_0$), derived from the stochastic model of canopy structure (Fig. 2). Panel a: BSFLA($\Omega\&\Omega_0$) as a function of zenith angle θ of the direction Ω (legend "BSFLA"). Zenith angle of Ω_0 is 41°. Also shown are VFLA(Ω) (legend "VFLA") and VFLA(Ω)VFLA(Ω_0) (legend "VFLA*SFLA"). Here $r/H=0.005$; $d=6366$; $u_L=\pi^2 d=0.5$. Panel b: Correlation coefficient of VFLA(Ω) and SFLA = VFLA(Ω_0) as a function of θ for relative leaf sizes $r/H=0.01$, 0.005 and 0.0025. Its definition is given in Appendix A.

sum of the escape probabilities for shaded and sunlit leaves, i.e., $\rho_{b,iso}(\Omega;\Omega_0)=[1-h_{iso}(\Omega;\Omega_0)]\rho_{iso}(\Omega)+h_{iso}(\Omega;\Omega_0)j_{iso}(\Omega;\Omega_0)$. Spherical integration of $\pi^{-1}\rho_{b,iso}(\Omega)|\mu|$ results in $(1-p_{b,iso})$ where $p_{b,iso}$ is the recollision probability. Some of the boundary scattered photons will escape the vegetation with unit probability. This lowers the probability for photons to recollide (i.e., $p_{b,iso}\le p_{iso}$) and consequently enhances the likelihood of photons escaping the vegetation (i.e., $\rho_{b,iso}(\Omega;\Omega_0)\ge\rho_{iso}(\Omega)$). Our next step is to demonstrate validity of these relationships in the general case of 3D heterogeneous canopy.

2.3. Generalization to 3D heterogeneous vegetation canopies

The goal of this section is to generalize our results presented in Sections 2.1 and 2.2. This will be done based on analyses of the stochastic radiative transfer equations (SRTE) (Appendix B). These equations accurately account for the canopy structure over a wide range of scale through the use of the pair-correlation function (Huang et al., 2008). Here we focus on the 3D vegetation canopy bounded from below by a non-reflecting surface. A physically based technique to account for contributions from reflecting canopy background will be detailed in Section 5 as part of our validation efforts.

Let the 3D vegetation canopy bounded from below by a non-reflecting surface be subjected to a monodirectional beam in the direction $-\Omega_0$. We represent the directions to the Sun, Ω_0, and sensor, Ω, by cosines of the sun, $\mu_0=\cos\theta_0$, and sensor, $\mu=\cos\theta$, polar angles, and their associated azimuths. The sunlit leaves in the direction Ω_0 form the canopy boundary. The incoming photons scattered by the boundary will interact with both shaded leaves and the boundary. The singly scattered photons that have not exited the canopy undergo the second interaction, resulting in a radiation field generated by photons scattered two times. A fraction of these photons in turn will recollide and give rise to a radiation field generated by photons scattered three times, etc. Let $I_m(z,\Omega)$ and F_m be the horizontal average radiance of radiation field generated by photons scattered m times and associated mean irradiance on leaf sides (Eq. (B2) in Appendix B.1), respectively. By definition (Fig. 1), the escape and recollision probabilities are $\rho_m(\Omega;\Omega_0)=\pi I_m(z_b,\Omega)/(\omega_\lambda F_{m-1})$ and $p_m=F_m/(\omega_\lambda F_{m-1})$. Here $z_b=0$ represents the upper horizonal surface above the canopy in the case of upward directions, and a surface beneath the canopy, $z_b=H$, for downward directions. Here symbols Ω and $-\Omega$ designate upward and downward directions. We start our analyses assuming that the foliage does not absorb radiation i.e., $\omega_\lambda=1$.

The Directional Area Scattering Function (DASF) is defined as the BRF of a vegetation canopy with non-absorbing leaves ($\omega_\lambda=1$) and bounded underneath by a non-reflecting surface (Knyazikhin et al., 2013). It can be expanded in successive order of scattering, or in Neumann series (Huang et al., 2007),

$$\begin{aligned}&\mathrm{DASF}(\Omega;\Omega_0)\mu_0\\&=\left[\rho_1(\Omega;\Omega_0)+\rho_2(\Omega;\Omega_0)\theta_1+\ldots+\rho_{m+1}(\Omega;\Omega_0)\theta_m^m+\cdots\right]i_0(\Omega_0),\end{aligned}\quad(5)$$

where $\theta_m=\sqrt[m]{p_1p_2\ldots p_m}$. The escape probability corresponding to the mth scattering order can be represented as

$$\rho_m(\Omega;\Omega_0)=[1-h_m(\Omega;\Omega_0)]\rho_{0m}(\Omega)+j_{iso}(\Omega;\Omega_0)h_m(\Omega;\Omega_0).\quad(6)$$

Here ρ_m and ρ_{0m} are escape probability densities for canopies with and without the stochastic boundary, respectively, and h_m is the correlation coefficient calculated as detailed in Appendix B.2. Integration of $\pi^{-1}\rho_m|\mu|$ over the unit sphere results in $1-p_m$ (Huang et al., 2007). The aim of this subsection is to understand relationships between ρ_{iso}, p_{iso}, ρ_m and p_m. Here we closely follow the theory documented in Huang et al. (2007). All calculations were performed using the stochastic radiative transfer equations.

Fig. 5 shows the escape, $\rho_m(\Omega;\Omega_0)$, and recollision, p_m, probabilities as functions of m. For view directions outside of the hot spot region, i.e., $h_m(\Omega;\Omega_0)\sim0$ and $\rho_m(\Omega;\Omega_0)\sim\rho_{0m}(\Omega)$, the escape probabilities for up- and downward directions vary with the number of successive scattering and reach plateaus from above and below after about 7–8 iterations (Fig. 5a). The semi-sum, $\overline{\rho}_m(\Omega;\Omega_0)=0.5[\rho_m(\Omega;\Omega_0)+\rho_m(-\Omega;\Omega_0)]$, saturates faster, after two to three scattering events in this example. The corresponding recollision probability p_m is related to $\overline{\rho}_m$ via Eq. (3) and thus it converges at the same or a faster rate. The limits $\overline{\rho}_m$ and p_m approximate $\rho_{b,iso}(\Omega)$ and $p_{b,iso}$. In the hot spot direction (Fig. 5b), i.e., when $\Omega\sim\Omega_0$ (and $h_m(\Omega;\Omega_0)\sim1$), the escape probability $\rho_m(\Omega;\Omega_0)$ is almost independent of the scattering order and approximates $j_{iso}(\Omega;\Omega_0)h_m(\Omega;\Omega_0)$, suggesting a negligible variation of h_m with m.

Fig. 6a shows an important feature of radiation fields corresponding to scattering orders at which the escape probability density saturates: $I_8(z,\Omega;\Omega_0)$ is proportional to $I_7(z,\Omega;\Omega_0)$, i.e., $I_8(z,\Omega;\Omega_0)=p_8I_7(z,\Omega;\Omega_0)$. It means that the radiative field generated by photons scattered 7 times is reduced by a factor p_8 as result of one interaction. The coefficient of proportionality is the recollision probability, i.e., $p_8=F_8/F_7$ (Huang et al., 2007). It follows from these relationships that $I_8(z,\Omega;\Omega_0)/F_8=I_7(z,\Omega;\Omega_0)/F_7$. This example illustrates a fundamental property of the 3D radiative transfer equation, i.e., the sequences $p_m=F_m/F_{m-1}$ and $e_m(z,\Omega;\Omega_0)=I_m(z,\Omega;\Omega_0)/F_m$, $m=1,2,\cdots$, converge to the unique

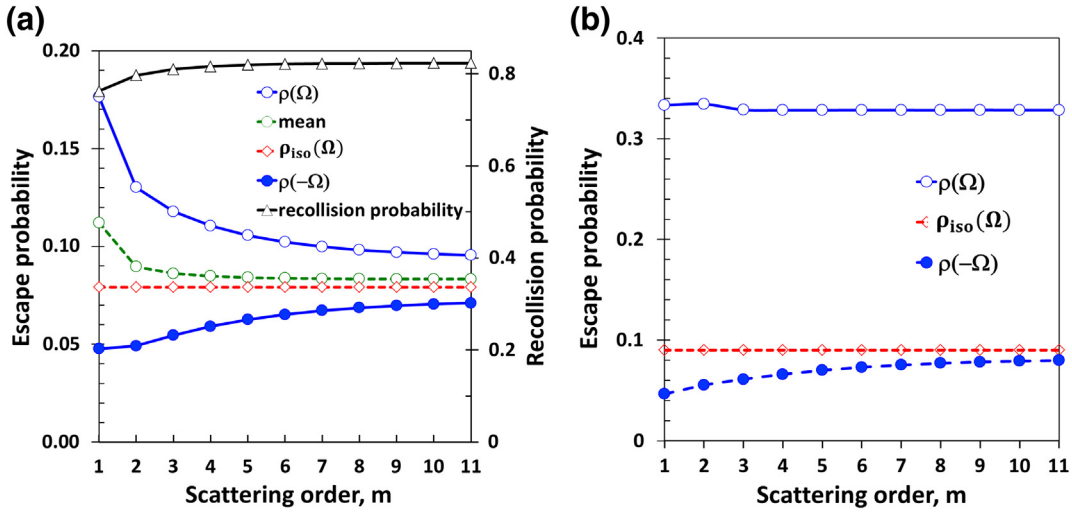

Fig. 5. Panel a: Directional escape probability densities in up-, $\rho_m(\Omega)$, and downward, $\rho_m(-\Omega)$, directions, their mean, $0.5[\rho_m(\Omega)+\rho_m(-\Omega)]$ (left axis), and recollision probability, p_m (right axis) for 11 scattering orders. Here solar zenith angle (SZA) and view zenith angle (VZA) are 41° and 49.1°, respectively. Panel b: Directional escape probabilities in up-, $\rho_m(\Omega)$, and downward, $\rho_m(-\Omega)$, directions for SZA = VZA = 49.1° and 11 scattering orders. $\rho_{iso}(\Omega)$ is shown on both plots. The stochastic radiative transfer equations were used to derive these variables. LAI = 5, ground cover was 0.8.

positive eigenvalue p_∞ of the radiative transfer equation, corresponding to the unique positive (normalized to unity) eigenvector $e_\infty(z,\Omega;\Omega_0)$ (Huang et al., 2007 Vladimirov, 1963). For a sufficiently large number of scattering events, the radiance $I_m(z,\Omega;\Omega_0)$ and, consequently, the escape probability density can be accurately approximated as $I_m(z,\Omega;\Omega_0)=p_\infty^m e_\infty(z,\Omega;\Omega_0)$ and $\rho_m(\Omega;\Omega_0)=p_\infty e_\infty(z_b,\Omega;\Omega_0)$. In this example e_m reaches its limit after 6–7 iterations, i.e., $I_m(z,\Omega;\Omega_0)=p_\infty^m e_7(z,\Omega;\Omega_0)$, and because p_m saturates after two to three scattering events (Fig. 5a), $p_\infty \approx \sqrt{p_1 p_2} \approx p_{iso}$. In general case the rate of convergence depends on p_∞: the higher its value, the slower the convergence (Huang et al., 2007).

Fig. 6b illustrates Eq. (6) for $m=7$. The boundary lowers the probability for photons to recollide and consequently enhances the likelihood of photons escaping the vegetation. This is seen in Fig. 6b: $\rho_m(\Omega;\Omega_0)$ differs from $\rho_{0m}(\Omega)$ by factor $(1-h_7)$ and therefore $\rho_m(\Omega;\Omega_0)\geq\rho_{0m}(\Omega)$. This yields an opposite inequality for the recollision probabilities. The escape probability densities $\rho_{0m}(\Omega)$ and $\rho_{0m}(-\Omega)$ converge to their limits almost symmetrically from above and below for all directions. Their semi-sum therefore approximates $\rho_{iso}(\Omega)$ for all directions, too. This is because the sensitivity of the term $\rho_{0m}(\Omega)$ to Ω_0 diminishes with the scattering order m. Its limit becomes independent on the direction of the incident beam in the case of canopies without stochastic boundary.

Solutions of the radiative transfer equation describe photons just before their interactions with scattering centers. In vegetation canopies it is radiance incident on the leaf surface. Distribution of photons just after their interactions is treated as distribution of sources on leaf surfaces, which is given by the source function (Eq. (B3) in Appendix B.1). Fig. 7a shows vertical profiles of the horizontal and angular averages of source functions, S_m, generated by the normalized radiance $e_m(z,\Omega)$ incident on leaf surfaces. Spherical integration of $e_m(z,\Omega)$ (as defined by Eq. (B3) in Appendix B.1) significantly lowers the angular variation in the source function (Davis and Knyazikhin, 2005 Knyazikhin et al., 2011). In this example the coefficient of angular variation of the source function (std/mean) is below 1.7% (Fig. 7b).

Thus, the scattering properties of the vegetation canopy are calculated as the sum of contributions from photons of different scattering orders (Eq. (5)). For sufficiently large m, the within canopy radiation regime is generated by spatially varying almost isotropic sources on leaf surfaces (Fig. 7). This feature makes the radiative regime similar

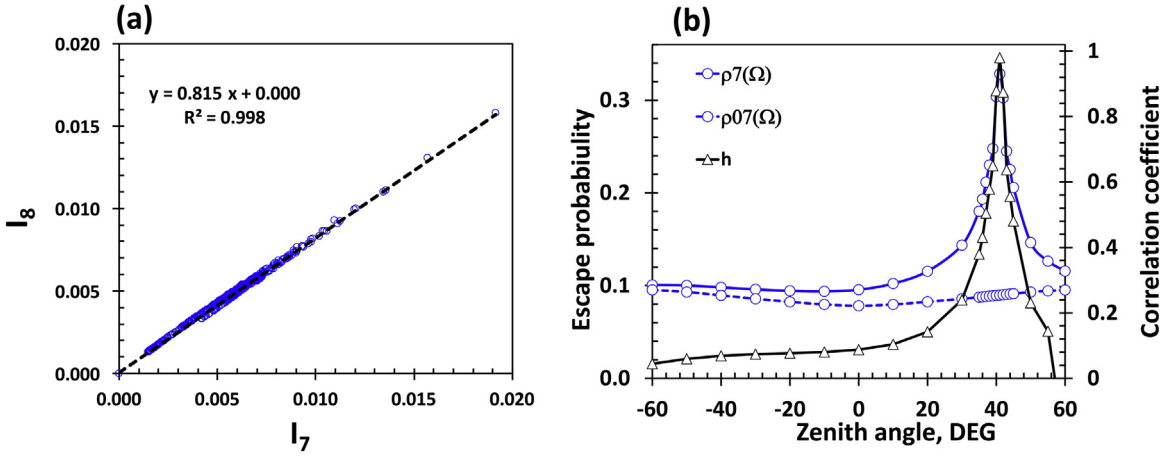

Fig. 6. Panel a: Relationship between $I_8(z,\Omega;\Omega_0)$ and $I_7(z,\Omega;\Omega_0)$ for $z=0,0.2,0.4,\cdots,1$ (in relative units) and 217 upward directions. Panel b: Escape probabilities $\rho_7(\Omega;\Omega_0)$, $\rho_{07}(\Omega)$ (vertical axis on the left side) and the correlation coefficient h_7 (vertical axis on the right side) in the principal plane as functions of view zenith angle of Ω. The probabilities are related as $\rho_7(\Omega;\Omega_0)=(1-h_7)\rho_{07}(\Omega)+h_7 j_{iso}(\Omega;\Omega_0)$ where the correlation coefficient h_7 was calculated as described in Appendix B.2. The stochastic radiative transfer equations with inputs as in Fig. 5 were used to derive these variables.

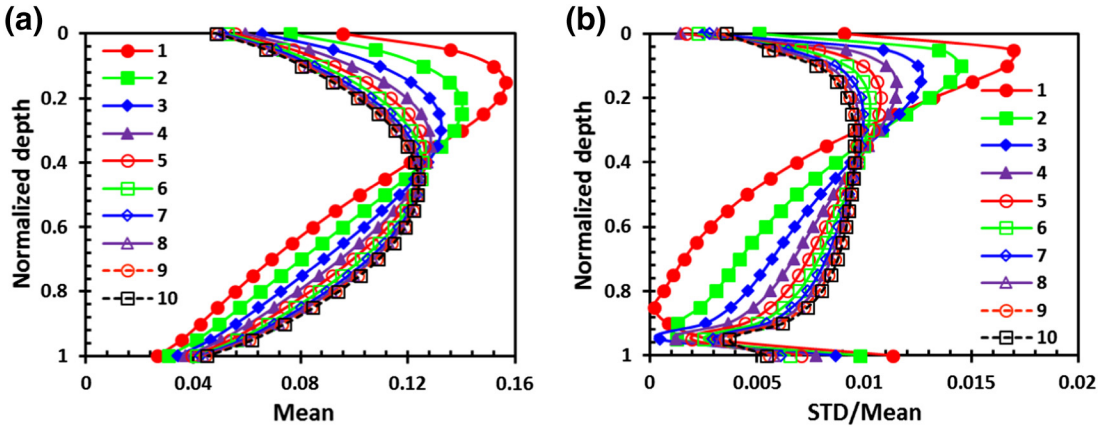

Fig. 7. Vertical profiles of horizontal and angular averages of source functions (panel a) and coefficient of variation (std/mean, panel b) due to radiative filed $e_m(z,\Omega)$ for 10 scattering orders. The dimensionless vertical axes show values of z/H where H is the canopy height. The stochastic radiative transfer equations with inputs as in Fig. 5 were used. The source function is defined by Eq. (B3).

to our simple model where the leaf-scattered radiation generates perfectly isotropic sources. Spatial variation of sources does not impact the recollision and escape probabilities. This is not true for low scattering orders. Our next step is to understand their impact on the average escape and recollision probabilities.

2.4. DASF and BRF

Based on Eq. (5) we define the average escape probability density as

$$\rho_A(\Omega;\Omega_0)=\sum_{m=1}^{\infty}\rho_m(\Omega;\Omega_0)w_{m-1}. \tag{7}$$

The weight $w_m=\theta_m^m/\sum_{k=0}^{\infty}\theta_k^k$, with θ_0 set to 1, accounts for the contribution of the mth scattering order. Because spherical integration of $\pi^{-1}\rho_m(\Omega)|\mu|$ results in $1-p_m$ for each m (Huang et al., 2007), the average escape probability also follows this relationship, i.e.,

$$\frac{1}{\pi}\int_{4\pi}\rho_A(\Omega;\Omega_0)|\mu|d\Omega=1-\sum_{m=1}^{\infty}p_m w_{m-1}=1-p_A, \tag{8}$$

where p_A is the average recollision probability (Stenberg, 2007 Stenberg et al., 2016). Note that the weight w_m can be expressed as $w_m=\theta_m^m(1-p_A)$. In terms of these notations the DASF takes the following form,

$$\mathrm{DASF}(\Omega;\Omega_0)=\frac{\rho_A(\Omega;\Omega_0)i_0(\Omega_0)}{1-p_A}. \tag{9}$$

The escape and recollision probabilities were introduced as conditional probabilities, i.e., they refer to photons that "survive" the scattering event (Fig. 1). The joint probabilities of recollision, escape and scattering events are $\omega_\lambda\rho_A$ and $\omega_\lambda p_A$. The BRF therefore becomes,

$$\mathrm{BRF}_\lambda(\Omega;\Omega_0)=\frac{\omega_\lambda\rho_A(\Omega;\Omega_0)i_0(\Omega_0)}{1-\omega_\lambda p_A}=\mathrm{DASF}\cdot W_\lambda(p_A), \tag{10}$$

where

$$W_\lambda(p_A)=\omega_\lambda\frac{1-p_A}{1-\omega_\lambda p_A}, \tag{11}$$

is the canopy scattering coefficient (Knyazikhin et al., 2013 Lewis and Disney, 2007 Smolander and Stenberg, 2005 Stenberg et al., 2016). Eq. (10) is the solution of the stochastic radiative transfer equations for the mean radiance formulated for a vegetation canopy bounded from below by a non-reflecting surface. We point out some features that are useful for developing inverse remote sensing techniques and their validation.

First, for vegetation canopies with a dark background or for sufficiently dense vegetation where the impact of the canopy background is negligible, the DASF and the scattering coefficient can be directly retrieved from the BRF spectrum without the use of canopy reflectance models, prior knowledge, or ancillary information regarding the leaf optical properties using a simple algorithm documented in Knyazikhin et al. (2013). The DASF, which is stored in the LUT, can be directly assessed using hyperspectral reflectance data acquired over dense canopies. We also use this algorithm to obtain the average escape and recollision probabilities from solutions of the stochastic radiative transfer equations (Appendix C).

Second, the decomposition Eq. (6) is also valid for the average escape probability density, i.e., ρ_A is a weighted sum of the averaged escape probability densities for shaded, $\rho_{0A}(\Omega)$, and sunlit, $j_{iso}(\Omega;\Omega_0)$, leaves. The DASF therefore can be represented as

$$\begin{aligned}\mathrm{DASF}(\Omega;\Omega_0)\mu_0&=[1-h(\Omega;\Omega_0)]\frac{\rho_{0A}(\Omega)i_0(\Omega_0)}{1-p_A}+h(\Omega;\Omega_0)\frac{j_{iso}(\Omega;\Omega_0)i_0(\Omega_0)}{1-p_A}\\&=[1-h(\Omega;\Omega_0)]\mathrm{DASF}_0(\Omega;\Omega_0)\mu_0+h(\Omega;\Omega_0)\mathrm{DASF}_b(\Omega;\Omega_0)\mu_0.\end{aligned} \tag{12}$$

Fig. 8a shows the average probabilities $\rho_A(\Omega;\Omega_0)$, $\rho_{0A}(\Omega;\Omega_0)$, and the correlation coefficient h. Our analyses suggest that the correlation coefficient varies insignificantly with scattering order (Fig. 5b). Fig. 8b reinforces this feature: the correlation coefficient derived from full solutions of the stochastic radiative transfer equations compares well with its 7th order approximation. This property has a simple physical interpretation. Indeed, photons scattered by the boundary toward the sun will escape vegetation with unit probability. Their amount depends on the boundary area, which in turn is determined by the canopy structure rather than within-canopy radiation regime.

Finally, the semi-sum $\overline{\rho}_{0m}(\Omega)$ and geometric mean θ_m of recollision probabilities converge to $\rho_{iso}(\Omega)$ and p_{iso} very fast (Fig. 5a). Approximating $\overline{\rho}_{0m}(\Omega)$ and θ_m in Eq. (7) by their limiting values, one obtains an approximation of the average semi-sum, i.e., $\overline{\rho}_{0A}(\Omega)(1-p_{iso})/(1-p_A)\approx\rho_{iso}(\Omega)$. For view directions outside of the hot spot region therefore the following relationship takes place,

$$\frac{\rho_{iso}(\Omega)}{1-p_{iso}}i_0(\Omega_0)\approx\frac{\overline{\rho}_A(\Omega)}{1-p_A}i_0(\Omega_0). \tag{13}$$

The left hand side of this equation is the Directional Area Scattering Factor, DASF_{iso}, in the case when leaves are subjected to isotropic radiation. This variable can be estimated from below canopy measurements

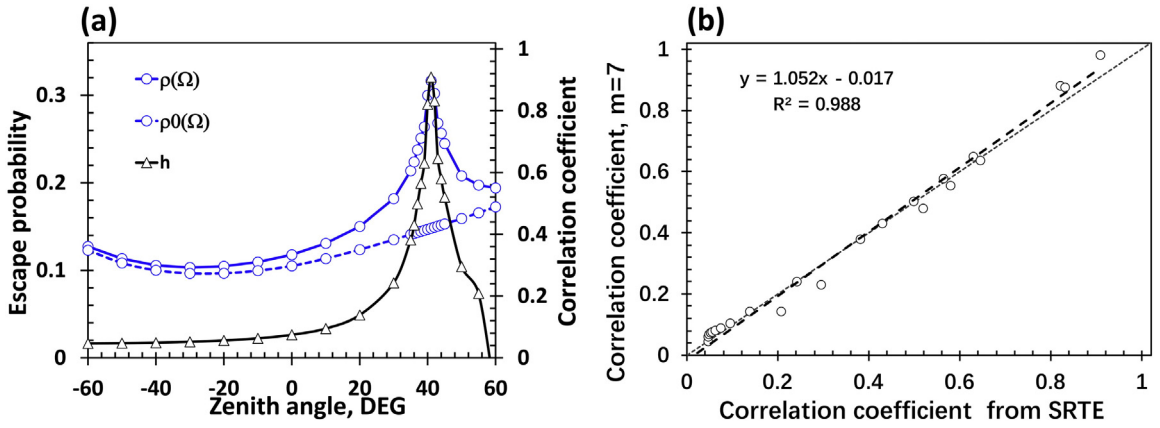

Fig. 8. Panel a: Average escape probabilities $\rho_A(\Omega;\Omega_0)$, $\rho_{0A}(\Omega)$ (vertical axis on the left side) and the correlation coefficient h (vertical axis on the right side) as functions of view zenith angle of Ω. Panel b: Comparison of the correlation coefficients derived from the SRTE (horizontal axis) and radiative field generated by photons scattered 7 times (vertical axis).

of the canopy directional uncollided transmittance using Eq. (4). Eqs. (1)–(4) therefore provide a basis for validation of the radiative transfer approach and assessments of retrieval techniques based on this approach.

Thus the BRF of a vegetation canopy bounded from below by a non-reflecting surface is expressed as a solution of the stochastic radiative transfer equations parameterized in terms of the measurable spectrally invariant parameters. This underlies our theoretical basis for developing LUT for the use with the DSCOVR EPIC data.

3. Study area and data used

3.1. Site description

This research is focused on Hyytiälä forest (Fig. 9) in the southern boreal zone in central Finland (61°50′N, 24°17′E). Dominant tree species are Norway spruce (*Picea abies*), Scots pine (*Pinus sylvestris*) and Silver birch (*Betula pendula*). Understory vegetation is classified as xeric, sub-xeric, mesic or herb-rich vegetation based on the species richness and abundance. The understory typically consists of two layers: the ground layer, which is mainly composed of mosses and lichens, and the upper layer, which is composed of, for example, dwarf shrubs and grasses. The growing season typically begins in early May and senescence in late August. Eighteen study sites representing different species and understory compositions were chosen for our analyses (Table 1). A detailed description of the study sites can be found in Heiskanen et al. (2013).

3.2. Field data

Data used in our research were sampled during peak growing season (June–July) on 18 locations (Fig. 9) in 2010 and 2012 (Lukeš et al., 2013 Rautiainen and Lukeš, 2015 Rautiainen et al., 2011).

The effective leaf area index and canopy directional uncollided transmittances were estimated from LAI-2000 Plant Canopy Analyzer data collected on selected locations between June 22 and July 4, 2010 when foliage had reached its maximum size. The measurements were taken shortly after (before) sunset (sunrise), or during overcast days, when forest was illuminated only by diffuse light. The sampling scheme was a cross with 12 measurement points: two perpendicular 6-point transects with 4-meter intervals between the measurement points. The forest measurements were made without view restrictors. The understory was excluded from the field of view since the measurements were taken at a height of 0.7 m. In addition to LAI-2000 measurements, stand basal area (BA), fractions of pine, spruce and birch trees (based on basal area), mean stem diameter at breast height (DBH), mean crown lengths and understory type for all 18 plots were measured (Table 1). The stand density was calculated as $BA/[\pi\cdot(0.5DBH)^2]$ (in stem/m^2). Angular profiles of canopy directional uncollided transmittances and effective LAI are shown in Fig. 10a. A detailed description of the measurements is documented in Heiskanen et al. (2012)and Rautiainen and Lukeš (2015).

Nadir hemispherical-conical reflectance factors (HCRF) of the understory in the spectral region from 325 nm to 1075 nm at spectral resolution of approximately 3 nm at 700 nm were measured between June

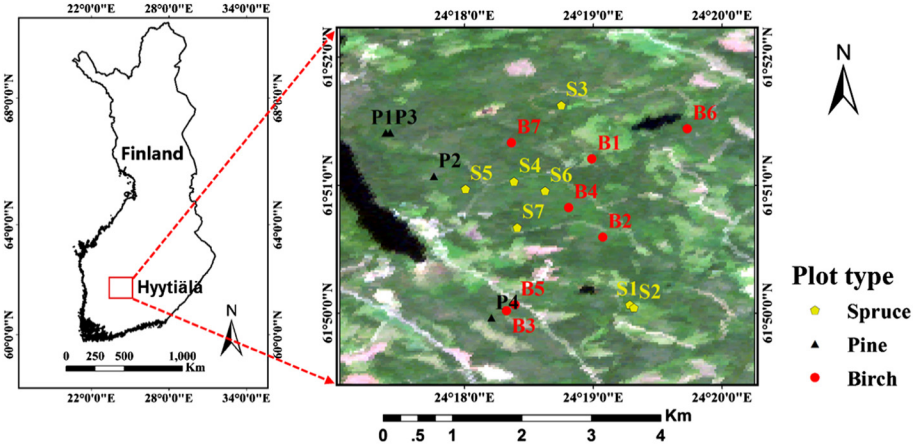

Fig. 9. Hyytiälä forest and distribution of study sites. The true color composite image is from Hyperion hyperspectral cube acquired on July 3, 2010.

Table 1
Species compositions, mean stem diameter at breast height (DBH), mean crown length, mean stand basal area (BA) and understory type for 18 plots in Hyytiälä forest. The Silver birch dominated site B7 and Norway spruce dominated site S4 are also treated as mixed forests.

Site ID	Scots pine, %	Norway spruce, %	Silver birch, %	DBH, cm	Crown length, m	BA, m^2/ha	Understory
B1	0	12.1	87.9	16.3	9.5	10.7	Mesic
B2	0	0	100.0	12.2	10.6	10.7	Herb-rich
B3	0	0	100.0	12.3	7.9	21.0	Mesic
B4	0	2.7	97.3	12.0	5.8	20.6	Herb-rich
B5	0	11.1	88.9	8.9	4.9	27.0	Herb-rich
B6	0	8.1	91.9	14.2	5.8	20.9	Mesic
B7	0	48.2	51.8	24.3	10.1	27.2	Mesic
P1	99.6	0.4	0	17.7	6.6	20.4	Mesic
P2	83.8	14.7	1.5	25.1	3.3	20.5	Sub-xeric
P3	95.2	1.5	3.2	20.0	8.6	24.3	Mesic
P4	65.4	26.9	7.7	24.3	6.2	26.0	Sub-xeric
S1	22.6	70.7	6.7	17.8	11	24.9	Mesic
S2	4.0	89.0	7.0	18.9	9.7	20.9	Mesic
S3	0.7	99.3	0	8.8	6.9	10.0	Mesic
S4	8.1	51.0	40.9	14.2	8.1	22.2	Mesic
S5	0	76.1	23.9	18.7	11.1	27.5	Mesic
S6	0	99.0	1.0	14.4	7.3	31.7	Mesic
S7	9.1	76.9	13.9	17.3	10.5	29.1	Xeric

29 and July 6, 2010 under diffuse light conditions using a FieldSpec UV/VNIR Spectroradiometer without fore-optics (i.e. the field-of-view was 25°). Forty measurement points were made for each understory type at intervals of 0.7 m on a 28 m long permanent transect. The ground area sampled at each point was approximately a circle with radius of 25 cm (Rautiainen et al., 2011). Spectra of understory HCRFs are shown in Fig. 10(b). Note that we follow standard reflectance nomenclature used in remote sensing (Martonchik et al., 2000 Schaepman-Strub et al., 2006)

Directional-hemispherical reflectance (DHRF) and transmittance (DHTF) of abaxial and adaxial sides of Norway spruce, Scots pine and Silver birch needles and leaves from the Hyytiälä forests were measured under laboratory conditions using ASD RTS-3ZC integrating sphere and ASD FieldSpec 3 PRO spectroradiometer in the spectral interval from 350 to 2500 nm with a spectral resolution of 3 nm at 700 nm and 10 nm at 1400 and 2100 nm between June 11 and 28, 2012 (Lukeš et al., 2013). Leaf albedo was calculated as sum of DHRF and DHTF. To measure conifer needle optical properties, the needles were secured in a special holder developed by Malenovský et al. (2006) at distances equal to or smaller than their thickness. The needle samples were scanned using a desktop document scanner, from which between-needle gap fractions were estimated using Otsu's automatic threshold method (Otsu, 1975). The gap fraction was used to correct DHRF and DHTF of conifer needles. A detailed description of this data set and measurement technique are documented in Lukeš et al. (2013). Mean spectra of leaf albedos used in our research are shown in Fig. 10(c). Maximum values of standard deviations were 0.029 (birch), 0.038 (pine) and 0.047 (spruce). The data are publicly available through the SPECCHIO database (Hueni et al., 2009).

3.3. Hyperion data

We used hyperspectral data from EO-1 Hyperion image (L1B product) acquired over the Hyytiälä forest on July 3, 2010. Hyperion is a narrowband imaging spectrometer that registers radiance in 242 spectral bands from 356 to 2577 nm, with about 10 nm bandwidth. Data spatial resolution is 30 m. The swath width is 7.7 km, and data are typically collected in 7.5 km by 100 km images (Pearlman et al., 2003). The striping, missing lines and spectral smile were removed from images or corrected using spectral moment matching (Sun et al., 2008), local destriping (Goodenough et al., 2003), interpolation and the pre-launch calibration measurements, respectively. The atmospheric correction was performed with the Fast Line-of-sight Atmospheric Analysis of Spectral Hypercubes (FLAASH) algorithm (Matthew et al., 2000). This technique results in an approximation of surface BRF. A detailed description of the processing of Hyperion images acquired over our study area can be found in Heiskanen et al. (2013) and Rautiainen and Lukeš (2015). The solar and view zenith angles were 41° and 13.8°; the relative azimuthal angle (RAA) of the Hyperion sensor was 62.73°. BRF spectra of pure Silver birch (B3), Scots pine (P1), Norway spruce (S3) and mixed (B7) plots are shown in Fig. 10(c). In our analyses, a plot was defined "pure" when at least 90% of the trees (by stem count) belonged to the given tree species.

4. Initialization of the stochastic radiative transfer equations

Structural variables that the stochastic radiative transfer equations admit include the conditional pair-correlation function, $K(z,\xi,\Omega)$, the fraction, $a(z)$, covered by tree crowns at depth z, and extinction coefficient, $\sigma(\Omega)$ (Appendix B.1). Our goal is to derive these variables from field data. We use analytical equations for K and a developed for mean tree crown idealized as a vertical solid, i.e., volume obtained by rotating a curve about the vertical axis (Huang et al., 2008). Under this assumption the conditional pair-correlation function and fraction $a(z)$ are explicit functions of the aspect ratio (crown length to crown diameter ratio) and stand density (Schull et al., 2011).

Specification of the extinction coefficient, $\sigma(\Omega)=u_L G(\Omega)$, requires effective leaf area volume density u_L (in m^2/m^3) and geometry factor $G(\Omega)$. The latter is determined by the type of leaf orientation (Ross, 1981 Stenberg, 2006). We use the inclination index of foliage area to parameterize the geometry factor (Ross, 1981). This index characterizes the deviation of leaf orientation from the spherical distribution and allows us to approximate the extinction coefficient for leaf and needle canopies as $\sigma(\Omega)=0.5\beta u_L$, where the weight β varies between 0 and 2. In the framework of the stochastic approach the effective leaf area volume density is related to the effective leaf area index, LAI, mean crown length, H_c, and stand density, d, as (Schull et al., 2011)

$$\mathrm{LAI}=u_L\int_0^{H_c}\{1-\exp[-d\pi r^2(z)]\}dz \tag{14}$$

Here $r(z)$ is the mean radius of the crown horizontal cross section at depth z, which in turn depends on the crown shape and aspect ratio (Schull et al., 2011).

Thus, data on stand density, d, mean crown length, H_c, leaf orientation, β, leaf area volume density, u_L, and crown aspect ratio, A, are needed to specify the coefficients that appear in the stochastic radiative transfer equations. The Norway spruce, Scots pine (Rautiainen et al., 2008) and Silver birch stands were idealized as forests consisting of ellipsoidal in shape trees. The stand density was calculated from the BA and DBH data as described in Section 3. The leaf area volume density can be estimated from Eq. (14) if the aspect ratio, crown length and effective LAI are known.

The site specific crown aspect ratio, A, and parameter β were estimated by selecting the most probable pair (A,β) for which angular profiles of canopy directional uncollided transmittance predicted by the stochastic radiative transfer equations (Eqs. (B1a) and (B1b) in Appendix B.1), agree with their measured counterparts (Fig. 10a) to within measurement uncertainties as follows. First, we expressed the effective leaf area volume density as a function of aspect ratio using Eq. (14) and measured effective LAI, stand density and mean crown length. Second, for each pair (A,β) we solved the stochastic radiative transfer equations for the directional uncollided transmittance (Appendix B.1) to obtain the angular profile of the directional uncollided transmittance as a function of the aspect ratio and leaf orientation. Next, we generated a set of acceptable solutions, which contained pairs (A,β) for which the RMSE between the modeled and measured profiles was below measurement uncertainty, which was

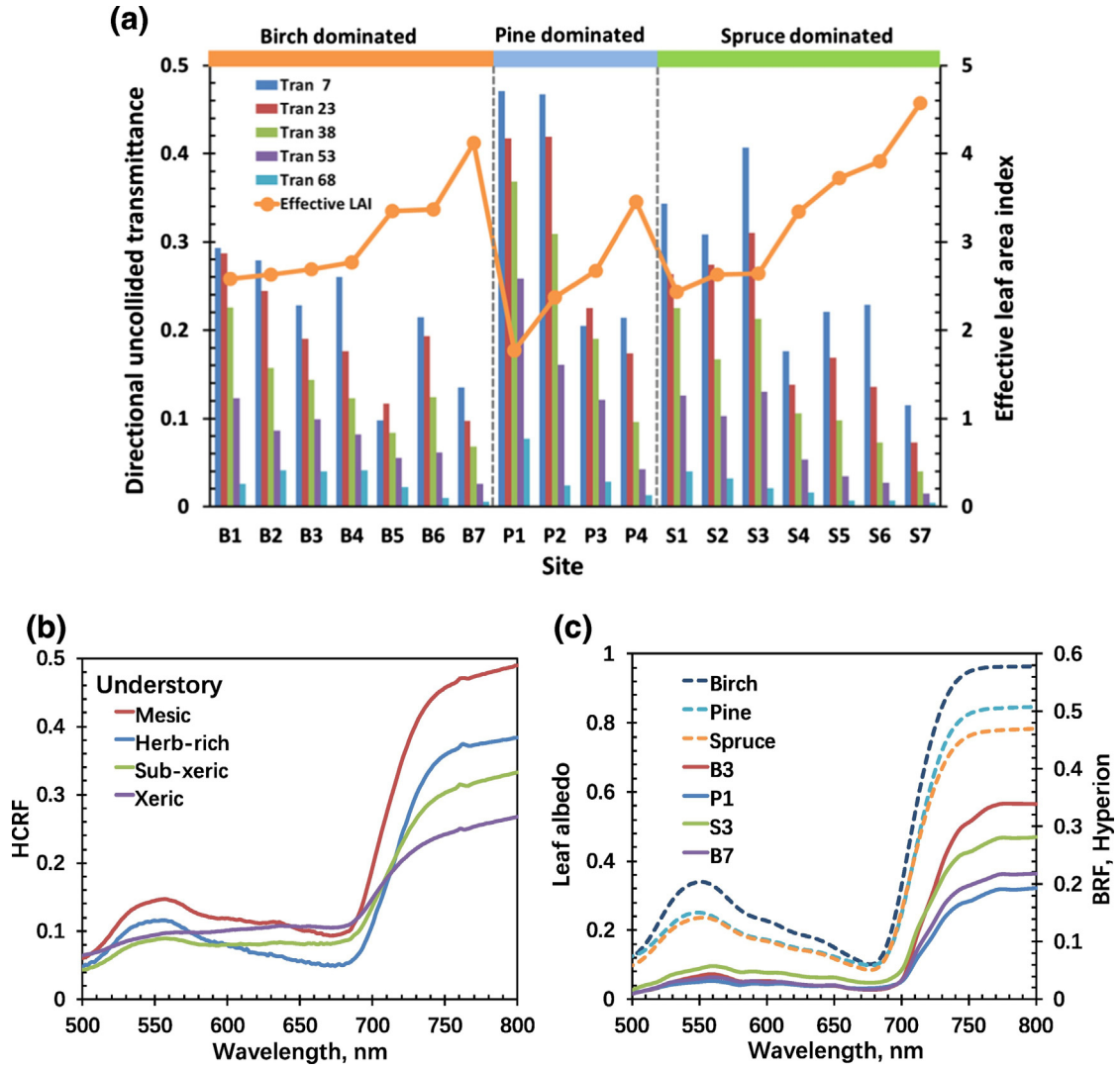

Fig. 10. Panel a: Angular profile of canopy directional uncollided transmittance (vertical axis on the left side) and effective leaf area index (vertical axis on the right side) for 18 locations (Table 1). Canopy directional uncollided transmittances are centered at five zenith angles: 7°, 23°, 38°, 53°, and 68° (legends "Tran 7" through "Tran 68"). Panel b: HCRF spectra of four understory types: herb-rich, mesic, sub-seric and xeric. Panel c: Leaf spectral albedo of Scots pine, Norway spruce needles, and Silver birch leaf (dashed lines, vertical axis on the left side). BRF spectra of pure Silver birch (B3), Scots pine (P1), Norway spruce (S3) and mixed (B7) plots (solid lines, vertical axis on the right side).

set to 0.025. Finally, we selected most probable pair (A,β) from histograms of the acceptable A and β values. This algorithm estimates mean within-crown extinction coefficient by correcting mean optical paths for crown geometry effects.

The above procedure was applied to each of 18 sites. Comparisons between simulated and predicted angular profiles suggest that the stochastic radiative transfer equations with the site specific structural parameters provide accurate estimates of the canopy directional uncollided transmittance (Fig. 11).

We used Eq. (13) to assess the ability of the stochastic radiative transfer equations to predict diffuse canopy radiation regime. The left hand side of this equation can be estimated from data on canopy directional uncollided transmittance, $t_0(\Omega)$ (Fig. 10a), which sums with the interceptance $i_0(\Omega)$ to unity, i.e., $i_0(\Omega) = 1 - t_0(\Omega)$, and the diffuse interceptance, i_{dif}, which is directly obtainable from the LAI-2000 Plant Canopy Analyzer readings (Rautiainen et al., 2009 Stenberg, 2007). It follows from Eq. (4) and (13) that $DASF_{iso} = 0.5(1 - t_0(\Omega))(1 - t_0(\Omega_0))/i_{dif}$. The right hand side of Eq. (13) can be estimated from solutions of the diffuse stochastic radiative transfer equations for vegetation canopy with non-reflecting leaves and bounded underneath by a non-reflecting surface (Section 2.4). Fig. 12 illustrates that the $DASF_{iso}$ predicted by the diffuse stochastic radiative transfer equations

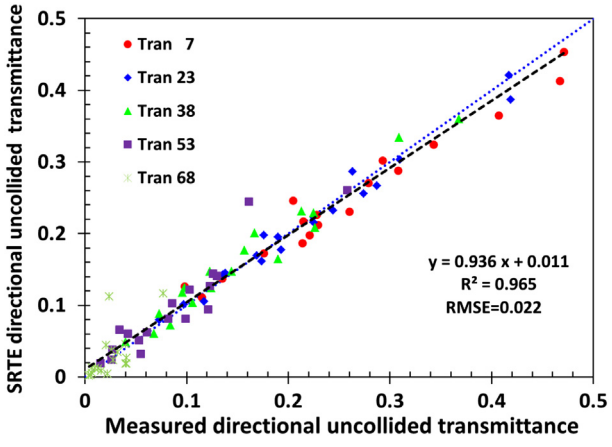

Fig. 11. Correlation between measured directional uncollided transmittances (horizontal axis) and predicted by the stochastic radiative transfer equations (vertical axis) for five zenith angles, 7°, 23°, 38°, 53° and 68° (legends "Tran 7" through "Tran 68") over 18 study plots.

with site specific structural parameters agree well with its measured counterpart.

Thus, we derived site specific wavelength independent extinction coefficients, conditional pair-correlation functions and vertical profiles of fraction covered by tree crowns, i.e., canopy structural variables that the stochastic radiative transfer equations require as input. These parameters are used in all our radiative transfer calculations.

5. Canopy-ground multiple interactions

The theoretical framework for the canopy BRF and DASF presented in Section 2 was developed under the assumption that the vegetation canopy is bounded from below by a non-reflecting surface. A radiative-transfer-based technique developed for the MODIS LAI/FPAR operational algorithm (Knyazikhin et al., 1998a) is adapted here to account for ground contributions.

The BRF of the vegetation canopy with a reflective ground can be represented as a sum of two components: the BRF calculated for the vegetation canopy with a non-reflecting underlying surface (termed as the "black soil" problem) and the contribution due to photon multiple interactions with canopy and ground, i.e.,

$$\mathrm{BRF}_\lambda(\Omega;\Omega_0) = \mathrm{BRF}_{BS,\lambda}(\Omega;\Omega_0) + \frac{r_\lambda}{1-r_\lambda \cdot R_{S,\lambda}} T_{BS,\lambda}(\Omega_0) I_{S,\lambda}(\Omega). \quad (15)$$

Here $T_{BS,\lambda}$ represents the total directional transmittance (uncollided and diffuse) for the black soil problem, and r_λ is the effective ground reflectance. The terms $I_{S,\lambda}(\Omega)$ and $R_{S,\lambda}$ are solutions of so-called "S problem," i.e, they represent canopy leaving radiance and downward reflectance if our canopy were illuminated from below by isotropic sources uniformly distributed over the canopy ground. Because $I_{S,\lambda}(\Omega)$ and $R_{S,\lambda}$ are solutions of the radiative transfer equation with non-reflecting ground, the spectral invariant approach presented in Section 2 is applicable to these terms. The BRF of the vegetated canopy with a reflective ground therefore can be expressed in terms of the wavelength dependent effective ground reflectance and leaf albedo, and spectrally invariant canopy interceptance, recollision and escape probabilities.

Results presented in Section 4 suggest that the stochastic radiative transfer equations can predict the canopy DASF, which a purely structural variable. Its estimation does not require information about leaf scattering properties. Specification of the basic structural element and its scattering coefficient is needed to estimate the canopy spectral BRF. In coniferous canopies, for example, clumped shoot structure causes multiple scattering within a shoot. The stochastic radiative transfer equations are not applicable at the needle scale because fluctuations of the number of needles in a shoot do not follow Poisson statistics. In radiative transfer models for conifers the shoot can be taken as the basic structural element (Smolander and Stenberg, 2003 Smolander and Stenberg, 2005). Its scattering coefficient, $\omega_{s,\lambda}$, is related to the needle albedo, $\omega_{0\lambda}$ as (Smolander and Stenberg, 2003 Smolander and Stenberg, 2005)

$$\omega_{s,\lambda} = \omega_{0\lambda} \frac{k_0}{1-p_0\omega_{0\lambda}}, \quad (16)$$

where the wavelength independent coefficients k_0 and p_0 depend on needle surface properties and their arrangement at a finer scale, i.e., within the shoot. The coefficients sum to unity if impact of needle surface properties can be neglected (Knyazikhin et al., 2013 Latorre-Carmona et al., 2014 Yang et al., 2016). The basic structural element can be associated e.g. with leaf, shoot, branch or tree crown. In all cases the relationship between their scattering coefficients and the leaf or needle albedo follows Eq. (16) where k_0 and p_0 account for the foliage distribution at a finer hierarchical level.

Solutions of the radiative transfer equation for the black soil and S problems have the form of Eq. (10). The canopy scattering coefficient, W_λ, is calculated using Eq. (11) with ω_λ representing the scattering coefficient of the basic structural element. The basic structural element specifies the recollision probability that appears in the canopy scattering coefficient W_λ. The DASF contains the ratio between the escape probability density and its spherical integral (see Eq. (9)). This makes this variable independent of the choice of the basic structural element (Eqs. (7) and (8) in Schull et al., 2011). The scaling properties of the scattering coefficient, recollision and escape probabilities underlie a technique to adjust retrieval algorithms for the sensor spatial resolution and spectral band composition (Ganguly et al., 2008b): the structural parameters can be pre-calculated at a fixed base scale (e.g., tree crown); the spectral BRF can be adjusted for the sensor resolution by transforming the measured leaf or needle albedo to the scattering coefficient of the basic structural element using Eq. (16) (Ganguly et al., 2008b).

In our case the tree crown is taken as the base scale. Leaves or needles are distributed within the crown in a certain fashion. We illustrate the technique outlined above to achieve consistency between the canopy scattering coefficient, within crown foliage arrangement and the spectral BRF at the Hyperion spatial resolution using data from the spectral interval between 710 and 790 nm. In this spectral interval albedo of any green leaf is related to a fixed spectrum via Eq. (16) (Knyazikhin et al., 2013 Latorre-Carmona et al., 2014 Schull et al., 2011 Yang et al., 2016) and thus two wavelength independent parameters, k_0 and p_0, suffice to specify the canopy scattering coefficient. The following algorithm was implemented. First, the spectrally invariant parameters were pre-calculated for the black soil and S problems using the stochastic radiative transfer equations with input collected at our sites. Note that the solution $I_{S,\lambda}(\Omega)$ of the S problem also have the form of Eq. (10) with the difference that spectrally invariant parameters p_A, ρ_A and i_0 are calculated assuming that our canopy is isotropically illuminated from below. Second, for each pair (k_s, p_0) the spectral BRF was calculated using scattering coefficient, $\omega_{s,\lambda}(k_s, p_0)$, obtained by transforming measured leaf albedo with Eq.(16), pre-computed structural parameters, and measured understory reflectance r_λ. Finally, we selected values of k_s and p_0 that minimized the RMSE between Hyperion and simulated BRF in the spectral interval between 710 nm and 790 nm. Fig. 13 illustrates proximity of the Hyperion and simulated BRF spectra for our 18 study plots.

To summarize, the spectral invariant approach is applicable in the general case of canopy reflective ground. The use of spectral invariants to parameterize the canopy spectral BRF makes the stochastic radiative transfer equations scalable, i.e., its solutions calculated at a fixed base scale can be adjusted for the sensor resolution and spectral band composition by changing the leaf or needle albedo with the spectrally invariant parameters unaltered.

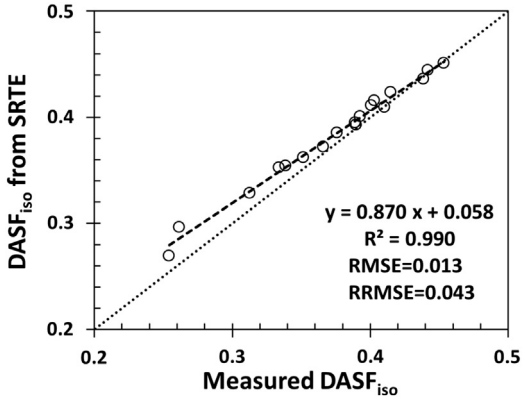

Fig. 12. Correlation between DASF_{iso} derived from field measurements (horizontal axis) and predicted by the stochastic radiative transfer equations (vertical axis) for the Hyperion sun-sensor geometry: SZA = 41°, VZA = 13.8° and RAA = 62.73°.

6. Discussion

We adapted retrieval approach implemented in the MODIS operational LAI/FPAR algorithm (Knyazikhin et al., 1998a Knyazikhin et al., 1998b). The algorithm compares measured spectral BRF with those evaluated from model-based entries stored in the LUT. All canopy structural variables and ground reflectance for which modeled and measured BRFs agree within uncertainties in the observed and modeled canopy reflectances are considered as acceptable solutions. The mean value of a structural variable of interest (e.g., LAI, VFLA and SLAI = LAI·VFLA) and its dispersion are taken as the solution of the inverse problem and its retrieval uncertainty. In addition to the measured BRFs, biome type and uncertainties in model and observations are also inputs to the algorithm (Wang et al., 2001). The LUT is a key element of the retrieval technique that determines its performance. Here we discuss differences between MODIS and EPIC LUTs.

Both LUTs are based on the representation of the modeled BRF via solutions of the black soil and S problems (Section 5), which are stored in the LUT. The EPIC LUT contains pre-calculated values of DASF, escape and recollision probabilities for the black soil and S problems, which correspond to various combinations of the sun-sensor geometry and canopy structural organization. The BRF for the black soil problem and solution of the S problem, $I_{S,\lambda}$, are calculated using Eq. (10). The spectral leaf albedo that appears in this equation becomes a biome-dependent configurable parameter that accounts for the sensor resolution and spectral band composition. Its specification is a part of the algorithm calibration and is based on analyses of the measured and simulated BRFs over validation sites representing various biome types as outlined in Section 5. Given sun-sensor geometry and biome type, the spectral BRF is modeled using Eq. (15), pre-calculated structural variables and spectral patterns of the effective ground reflectance (which are also stored in the LUT).

Note that Eq. (10) not only provides a highly accurate approximation of solutions of the radiative transfer equations for vegetation canopies with non-reflecting ground, but also follows scaling relationships between the basic structural element, its scattering spectrum and spectral BRF. This feature underlies the scale-dependent formulation of the radiative transfer process in vegetation canopies. The spectrally invariant relationships for canopy transmittance, absorptance and reflectance used in various process oriented models (Stenberg et al., 2016) are special cases of Eq. (15) that naturally follow from its hemispherical integrations (Huang et al., 2007).

The MODIS LUT stores the ratio between BRF and directional hemispherical reflectance (DHR) at a fixed wavelength for the black soil and S problems as a function of the sun-sensor geometry and canopy structure (Knyazikhin et al., 1998a Knyazikhin et al., 1998b). The spectral DHR is expressed via spectral canopy transmittance and absorptance, which in turn are calculated using spectrally invariant relationships for the canopy transmittance and absorptance. The BRF is assembled using Eq. (15), pre-calculated ratio, spectral DHR and patterns of the effective ground reflectance. The biome dependent spectral leaf albedo is also configurable parameter that controls consistency between the basic structural element and canopy spectral transmittance and absorptance at the sensor spatial resolution. The scaling properties however are not fully realized in the MODIS LUT because the spectrally invariant relationships are utilized only for the special cases of canopy reflectance and transmittance. This results in higher model uncertainties due to adjustments of the LUT for the sensor characteristics compared to the EPIC LUT.

Another important distinction between the EPIC and MODIS LUTs is that the former accounts for the stochastic boundary whereas the latter assumes infinitesimal scatters. The MODIS LUT based algorithm does not perform retrievals if the view direction falls within the hot spot region. Recall that DASF for the vegetation canopy with the stochastic boundary is a weighted sum of $DASF_0$ calculated assuming infinitesimal scatters and $DASF_b$ of the stochastic boundary (Eq. (12)). The EPIC LUT incorporates this decomposition, i.e., it contains $DASF_0$, $DASF_b$ and the correlation coefficient h. The correlation coefficient depends on a model used to simulate the hot spot effect. This feature allows for integration of various hot spot models into the retrieval technique without recalculating $DASF_0$ and $DASF_b$.

The parameterization of the LUT in terms of structural variables obtainable from both space and ground measurements is the key advantage of the EPIC LUT over its MODIS counterpart. For example, for vegetation canopies with a dark background or for sufficiently dense vegetation where the impact of the canopy background is negligible, the DASF can be directly retrieved from the BRF spectrum in the 710 to 790 nm interval without the use of canopy reflectance models, prior knowledge, or ancillary information regarding the leaf optical properties using a simple algorithm documented in Knyazikhin et al. (2013). The DASF can be compared with LUT entries. In general case the removal of the ground contribution to BRF should precede retrieval of DASF. Eq. (15), which is incorporated in the LUT, provides physical basis for removing ground influences from measured spectral BRF. The field and hyperspectral data therefore can be used to assess the EPIC LUT, to diagnose its deficiencies and to develop refinements. We illustrate this feature using field data and hyperspectral images.

First, we used the pre-calculated site specific spectral invariants for the black soil and S problems (Section 4), measured ground reflectance and the sensor adjusted leaf albedo to evaluate the term in Eq. (15) that accounts for ground contributions. This term was subtracted from the Hyperion BRF to estimate $BRF_{BS,\lambda}(\Omega;\Omega_0)$. We applied the algorithm reported in Knyazikhin et al. (2013) to $BRF_{BS,\lambda}$ to derive Hyperion $DASF(\Omega;\Omega_0)$ (Appendix D) over our study sites. The view direction of

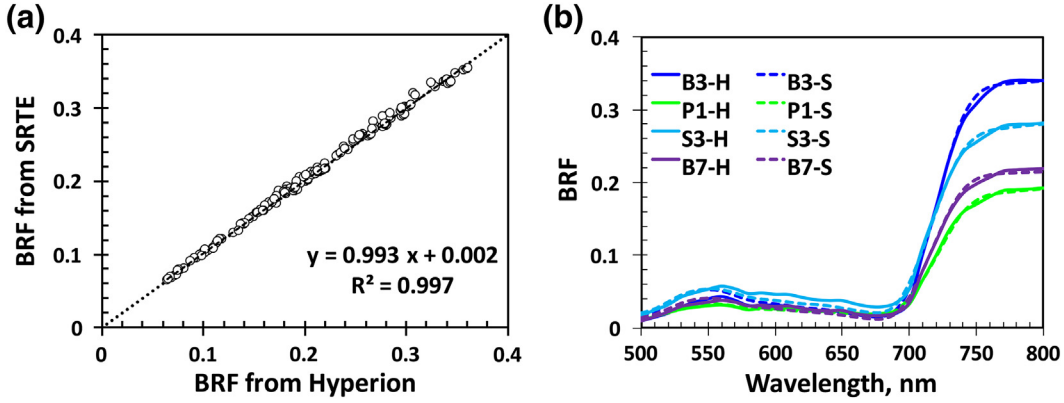

Fig. 13. Panel a: Correlation between Hyperion $BRF_{H,\lambda}(\Omega)$ and SRTE-estimated $BRF_\lambda(\Omega)$ in the 710- to 790 nm spectral interval for 18 study plots. Panel b: Simulated (dashed lines) and Hyperion (solid lines) BRF spectra of pure Silver birch (B3), Scots pine (P1), Norway spruce (S3) and mixed (B7) forests. The RMSE (and R^2) for the 500 to 700 nm interval are 0.007 (0.845), 0.003 (0.831), 0.005 (0.778) and 0.004 (0.807), respectively. The remaining sites showed similar behavior.

the Hyperion sensor was outside of the hot spot region (i.e., $h(\Omega;\Omega_0)\approx 0$) and thus the retrieved DASF provides an estimate of $DASF_0$ in the direction to the sensor.

Next, we calculated DASF in the direction $-\Omega$ using the stochastic radiative transfer equations and site specific canopy structural parameters. The simulated and Hyperion DASFs were then used to evaluate $DASF_{iso}$ as the semi-sum of their values for up- and downward directions. The correlation between $DASF_{iso}$ derived from Hyperion images and field data shown in Fig. 14 suggests that the modeled DASF is accurate for our broad- and needle leaf dominant forest sites at the Hyperion resolution and LAI range between 2 and 5.

Finally, we estimated $i_0(\Omega)$ from Eq. (4) as $i_0(\Omega) = 2DASF_{iso} i_{dif}/i_0(\Omega_0)$ with the ratio $i_{dif}/i_0(\Omega_0)$ calculated using the stochastic radiative transfer equations and site specific canopy structural parameters. The canopy interceptance in the direction Ω was then converted to VFLA(Ω) with Eq. (1). The VFLA(Ω) can also be directly estimated from below canopy measurements of the canopy directional uncollided transmittance. The correlation between VFLA derived from field measurements and Hyperion image shown in Fig. 15 suggests the LUT developed for our sites provides an accurate relationship between canopy BRF and VFLA at the Hyperion resolution and consequently supports our theoretical basis.

7. Concluding remarks

This paper presents the theoretical basis of the algorithm designed for the generation of leaf area index and its sunlit fraction from NASA's EPIC instrument onboard NOAA's DSCOVR spacecraft. The algorithm ingests spectral surface BRF data, canopy architectural type (or biome), model and observation uncertainties. The technique used in the MODIS LAI/FPAR operational algorithm is adapted to select most probable values of LAI, SFLA, SLAI = SFLA·LAI and their uncertainties. The use of spectral invariants in the parameterization of the MODIS LUT imbued scale dependency to the algorithm, which is among key requirements to generate long-term records of biophysical parameters from remote sensing measurements of multiple sensors (Ganguly et al., 2008a Ganguly et al., 2008b). The theoretical basis of the MODIS LUT however has not been revised since 1998 when the first spectrally invariant parameter, maximum eigenvalue of the radiative transfer equation, was originally introduced (Knyazikhin et al., 1998a Knyazikhin et al., 1998b). The purpose of our study has been to modify the LUT through incorporations of the canopy hot spot phenomenon and recent advances in the theory of canopy spectral invariants (Stenberg et al., 2016) and to integrate the retrieval of the VFLA into the MODIS algorithm. The modifications improve decoupling of the structural and radiometric components of the BRF and algorithm scaling properties,

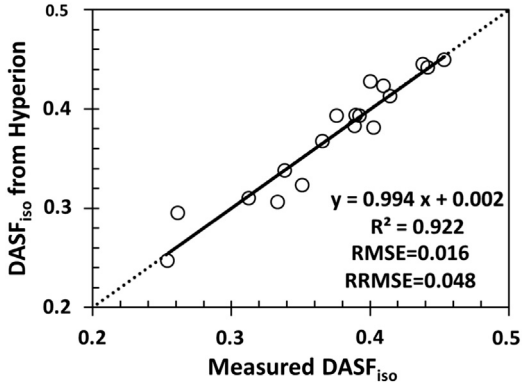

Fig. 14. Correlation between $DASF_{iso}$ derived from field measurements (horizontal axis) and Hyperion image (vertical axis) for 18 study sites. Here SZA = 41°, VZA = 13.8° and RAA = 62.73°.

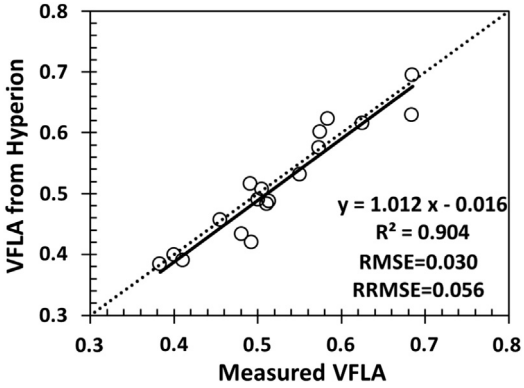

Fig. 15. Correlation between VFLA derived from field measurements (horizontal axis) and Hyperion image (vertical axis) for 18 study sites. Here SZA = 41°, VZA = 13.8° and RAA = 62.73°.

which are important prerequisites for achieving consistency and complementarity between DSCOVR EPIC and existing satellite derived land surface biophysical parameters. The stochastic radiative transfer equations are used to generate the EPIC LUT for all biome types. The equations naturally account for the effects of the three-dimensional canopy structure on the BRF and therefore an accurate discrimination between sunlit and shaded leaf areas is expected. The entries of the EPIC LUT are measurable, i.e., they can be independently derived from both below canopy measurements of the transmitted and above canopy measurements of reflected radiation fields. This is the key advantage of the EPIC LUT over its MODIS counterpart because this feature makes possible direct validation of the LUT, facilitates identification of its deficiencies and development of refinements. Analyses of field data and hyperspectral images suggest that the EPIC LUT accurately follows regularities expected from the theory.

Acknowledgment

This research was funded by the NASA DSCOVR project under grant NNX15AB11G. B. Yang and L. Yan were supported in part by the National Natural Science Foundation of China No. 41371492, Doctoral Program No. 20130001110046 and Chinese Scholarship Council No. 201406010058. M. Mõttus and M. Rautiainen were supported by the Academy of Finland under grants 266152 and 13286390, respectively.

Appendix A. Stochastic model of canopy structure and radiation regime

We use the Boolean model of random set to simulate 3D canopy structure (Stoyan et al., 1995). The following stationary Poisson germ-grain stochastic process of intensity d (in number per volume) is implemented. A random number $k = dV$ of leaves within a volume $V = HS$ is selected using the Poisson distribution $P(k) = (\bar{k})^k \exp(-\bar{k})/k!$ where $\bar{k}$ is the mean value of the random variable k. Random locations of k leaves in V are generated with a uniform distribution function. On each of these points a disc of radius r (Fig. 2b) is placed. Their random orientation is generated with a leaf normal distribution function $g_L(\Omega_L)$. The volume V with k randomly oriented leaves (Fig. 2a) is a realization of the canopy structure. The leaf area volume density of the canopy realization is $\pi r^2 k/V$. Its ensemble average value results in $u_L = \pi r^2 d$. In the terminology the points of the Poisson process are the germs while the discs represent the grains (Stoyan et al., 1995).

The discs simulate bi-Lambertian leaves, i.e., the incident photons are reflected from, or transmitted though, the disc in a cosine distribution about its normal. Its scattering properties are parameterized in terms of leaf transmittance, τ_L, and reflectance, r_L. Their sum is the leaf albedo, $\omega = \tau_L + r_L$. The leaf normal distribution function for spherically oriented leaves is $g_L(\Omega_L) = 1$. For non-spherically oriented leaf normal

$\Omega_L=(\theta_L,\varphi_L)$, a trigonometrical representation of $g_L(\Omega_L)$ is used (Bunnik, 1978), i.e.,

$$g_L(\Omega_L)=\frac{2}{\pi}\left(\frac{1+a\ \cos b\theta_L}{\sin\theta_L}\right). \tag{A1}$$

This model includes planophile ($a=1,b=2$), erectophile ($a=-1,b=2$), plagiophile ($a=-1,b=4$), extremophile ($a=1,b=4$) and uniform ($a=0$) leaves.

Each disc is divided into n equal sub-areas $s_0=\pi r^2/n$, which represents smallest resolvable scale (Fig. 2b). The bi-Lambertian scattering is simulated for each sub-area s_0. The disc radius is expressed relative to the canopy height H, i.e., $r/H=\alpha$. We define the indicator function $\chi(\mathbf{x},\Omega)$ of gaps such that it is 1 if there is a free line of sight through the canopy from the point $\mathbf{x}$ on a sub-area s_0 in the direction Ω, and 0 otherwise (Stenberg, 2007). Since the canopy structure is treated as a stochastic process, the gap distribution $\chi(\mathbf{x},\Omega)$ is a stochastic function of space. Its ensemble average value describes gap density per unit solid angle per unit leaf area.

For each realization of canopy structure and a set of N_Ω directions distributed on a unit sphere, we count photons that recollide, $N'=\sum_{\mathbf{x},\Omega}[1-\chi(\mathbf{x},\Omega)]|\Omega\cdot\Omega_L(\mathbf{x})|$ and exit the canopy through gaps along the direction Ω, $M(\Omega)=\sum_{\mathbf{x}}\ \chi(\mathbf{x},\Omega)|\Omega\cdot\Omega_L(\mathbf{x})|$. Realizations of the total leaf semi-surface area, A_T, their visible, $A_V(\Omega)$, shaded, $A_{sh}(\Omega\neg\Omega_0)$, and bi-directional sunlit, $B(\Omega\&\Omega_0)$, areas were estimated as $A_T=s_0kn$, $A_V(\Omega)=s_0\sum_{\mathbf{x}}\ \chi(\mathbf{x},\Omega)$, $A_{sh}(\Omega\neg\Omega_0)=s_0\sum_{\mathbf{x}}\chi(\mathbf{x},\Omega)(1-\chi(\mathbf{x},\Omega_0))$, and $B(\Omega\&\Omega_0)=s_0\sum_{\mathbf{x}}\chi(\mathbf{x},\Omega)\chi(\mathbf{x},\Omega_0)$. Ensemble average values of these random variables were assigned to the recollision, $p_{iso}=\langle N'\rangle/\langle A_T\rangle$ and escape $2\rho_{iso}(\Omega)=\langle M(\Omega)\rangle/\langle A_T\rangle$ probabilities, $\mathrm{VFLA}(\Omega)=\langle A_V(\Omega)\rangle/\langle A_T\rangle$, $\mathrm{VFLA}_{sh}(\Omega\neg\Omega_0)=\langle A_{sh}(\Omega)\rangle/\langle A_T\rangle$, $\mathrm{BSFLA}(\Omega\&\Omega_0)=\langle B(\Omega\&\Omega_0)\rangle/\langle A_T\rangle$, and $i_0(\Omega)=\langle M(\Omega)\rangle/(S\mu)$. Here $\langle\cdot\rangle$ designates ensemble averaging, i.e., over all realizations of canopy structure in V. The correlation coefficient of $\mathrm{VFLA}(\Omega)$ and $\mathrm{SFLA}=\mathrm{VFLA}(\Omega_0)$ was calculated as

$$h_{iso}(\Omega;\Omega_0)=\frac{\mathrm{BSFLA}(\Omega\&\Omega_0)-\mathrm{VFLA}(\Omega)\mathrm{VFLA}(\Omega_0)}{\sqrt{\left[\mathrm{VFLA}(\Omega)-\mathrm{VFLA}^2(\Omega)\right]\left[\mathrm{VFLA}(\Omega_0)-\mathrm{VFLA}^2(\Omega_0)\right]}} \tag{A2}$$

From simulations, the joint probability $\mathrm{VFLA}_{sh}(\Omega\neg\Omega_0)$ was found to be equal to $[1-h_{iso}(\Omega;\Omega_0)]\mathrm{VFLA}(\Omega)(1-\mathrm{VFLA}(\Omega_0))$, as expected. We introduce a fraction of shaded leaves visible outside the canopy along a given direction $-\Omega$ as the conditional probability of seeing a shaded leaf under the condition that the leaf area does not belong to the canopy boundary, i.e $\mathrm{VFLA}_{sh}(\Omega;\Omega_0)=\mathrm{VFLA}_{sh}(\Omega\neg\Omega_0)/(1-\mathrm{VFLA}(\Omega_0))=(1-h(\Omega;\Omega_0))\mathrm{VFLA}(\Omega)$.

The joint probability that a photon scattered by the boundary and escape the vegetation was calculated as $\langle\sum_r\chi(\mathbf{x},\Omega)\chi(\mathbf{x},\Omega_0)|\Omega\cdot\Omega_L(\mathbf{x})||-\Omega_0\cdot\Omega_L(\mathbf{x})|\rangle/\langle A_T\rangle$. From simulations, this probability was found to be equal to $\mathrm{BSFLA}(\Omega\&\Omega_0)\Gamma(\Omega_0\to\Omega)/G(\Omega_0)$, as expected, where G and Γ are the geometry factor and area scattering phase function, respectively (Ross, 1981). The conditional probability density by which a photon scattered by the boundary will escape the vegetation in the direction Ω is $j_{iso}(\Omega;\Omega_0)=\Gamma(\Omega_0\to\Omega)/G(\Omega_0)$. It describes number of canopy leaving photons per unit sunlit area (i.e., per unit boundary area). The escape probability, $\rho_{b,iso}(\Omega;\Omega_0)$, for the stochastic model with the boundary in the direction Ω_0 can therefore be represented as $\rho_{b,iso}(\Omega;-\Omega_0)=(1-h_{iso}(\Omega;\Omega_0))\rho_{iso}(\Omega)+j_{iso}(\Omega;\Omega_0)h_{iso}(\Omega;\Omega_0)$. Solving this equation for h_{iso} one obtains

$$h_{iso}(\Omega;\Omega_0)=\frac{\rho_{b,iso}(\Omega;\Omega_0)-\rho_{iso}(\Omega)}{j_{iso}(\Omega;\Omega_0)-\rho_{iso}(\Omega)} \tag{A3}$$

We use this equation to evaluate the correlation coefficient from solutions of the stochastic radiative transfer equations as detailed in Appendix B.2.

Appendix B. Stochastic radiative transfer equations

B.1. Ensemble average intensity and its second moment

Let a stochastic canopy resided in the layer $0\le z\le H$ be subjected to a monodirectioanl beam in the direction $\Omega_0=(\theta_0,\varphi_0)$ of intensity L_0. Vertical profiles of the horizontal average intensity, $I(z,\Omega)$, and its second moment, the mean intensity incident on the leaf surface, $U(z,\Omega)$, at depth z satisfy a system of stochastic equations (Huang et al., 2008). The vertical profiles, $L_0I_0(z)\delta(\Omega-\Omega_0)$ and $L_0U_0(z)\delta(\Omega-\Omega_0)$, of the uncollided (direct) intensities in the direction Ω_0 are solutions of the following equations,

$$I_0(z)+\frac{\sigma(\Omega_0)}{\mu_0}\int_0^z a(\xi)U_0(\xi)d\xi=1, \tag{B1a}$$

$$U_0(z)+\frac{\sigma(\Omega_0)}{\mu_0}\int_0^z K(z,\xi,\Omega_0)U_0(\xi)d\xi=1. \tag{B1b}$$

Here $\mu_0=\cos\theta_0$; $\sigma(\Omega)$ denotes the extinction coefficient; $a(\xi)$ is the probability of finding a foliated point at depth ξ, and $K(z,\xi,\Omega)$ represents the conditional pair-correlation function, i.e., $a(z)K(z,\xi,\Omega)$ is the probability of finding simultaneously foliated points at depths z and ξ along a given direction Ω (Huang et al., 2008 Vainikko, 1973). The conditional pair-correlation function describes spatial correlation between phytoelements, e.g., clumping of leaves into branches, branches into crowns, etc. If leaves are not spatially correlated ($K=a(\xi)$), Eqs. (B1a) and (B1b) coincide and their solutions are the Beer-Lambert law. Equations for diffuse components and various models of a and K can be found in Huang et al. (2008).

Solution of Eqs. (B1a) and (B1b) at the canopy bottom, $z=H$, is the canopy directional uncollided transmittance in the direction Ω_0. This variable can be estimated from measurements of downward fluxes below and above the canopy using the LAI-2000 plant analyzer (Rautiainen et al., 2009 Rautiainen and Stenberg, 2015 Stenberg, 2007). The canopy interceptance is then $i_0(\Omega_0)=1-I_0(H)$.

The mean irradiance on leaf sides, F, and source function, S, are given by

$$F=\int_0^H\int_{4\pi}\sigma(\Omega)a(z)U(z,\Omega)dzd\Omega, \tag{B2}$$

$$S(z,\Omega)=\frac{1}{\pi}\int_{4\pi}P(\Omega'\to\Omega)\sigma(\Omega')U(z,\Omega')d\Omega' \tag{B3}$$

where $P(\Omega'\to\Omega)=\Gamma(\Omega'\to\Omega)/G(\Omega')$. We use the stochastic radiative transfer equations to simulate BRF of vegetated surface. The method of successive orders of scattering approximation was used to numerically solve the system for the diffuse components as well as to estimate terms in Neumann series (Eq. (5)).

B.2. Correlation coefficient

The radiative transfer equation is formulated for interior points in the domain in which the radiative transfer process occurs. The shaded leaves represent the interior points. To exclude the stochastic boundary from the domain the leaf area volume density is represented as $u_L[1-c_{HS}(\Omega;\Omega_0)]$ where c_{HS} is a hot spot parameter that accounts for the statistical dependency of seeing gaps in the direction Ω from the sunlit areas of leaves. We followed (Kuusk, 1991) techniques to evaluate this parameter. The escape probability density, $\rho(\Omega;\Omega_0)$, derived from solutions of the boundary value problem for the radiative transfer equation accounts for both photons scattered by shaded and sunlit leaf areas. If

c_{HS} is set to zero the corresponding escape probability density, $\rho_0(\Omega)$, quantifies the escape event due to photon interactions with shaded leaves. In this case the equation acts in much the same way as we estimate the probabilities in Section 2.1, i.e., it assumes that there are no points on leaf surfaces from which photons can escape the vegetation with unit probability. The correlation coefficient h can be estimated from Eq. (A3) in which $\rho(\Omega;\Omega_0)$ and $\rho_0(\Omega)$ are used in place of $\rho_{b,iso}(\Omega;\Omega_0)$ and $\rho_{iso}(\Omega)$. Its specification requires to solve the stochastic equations two times, first with an actual c_{HS} to get $\rho_b(\Omega;\Omega_0)$, and then with c_{HS} set to zero in order to obtain $\rho_0(\Omega)$.

Appendix C. Estimation of average escape and recollision probabilities

It follows from Eq. (10) that the ratio $\mathrm{BRF}_\lambda(\Omega;\Omega_0)/\omega_\lambda$ is linearly related to $\mathrm{BRF}_\lambda(\Omega;\Omega_0)$ where slope and intercept give p_A and $\rho_A(\Omega;\Omega_0)i_0(\Omega_0)$. We use this obvious property to specify the average recollision and escape probabilities as follows: solve stochastic radiative transfer equations for several values of leaf albedo first and then specify slope and intercept from the $\mathrm{BRF}_\lambda(\Omega;\Omega_0)/\omega_\lambda$ vs. $\mathrm{BRF}_\lambda(\Omega;\Omega_0)$ linear relationship. The slope is the average recollision probability. The average escape probability is the ratio between the intercept and $i_0(\Omega_0)$. The escape probability can be decomposed into contributions from shaded and sunlit leaves as described in Sect. B2.

Appendix D. Retrieving DASF from hyperspectral BRF

The algorithm for the estimation of DASF from the BRF spectrum in the 710 to 790 nm interval uses the transformed reference leaf albedo $\varpi_{0\lambda}$, which is related to the sensor-adjusted leaf albedo, $\omega_{s,\lambda}$, as (Knyazikhin et al., 2013)

$$\omega_{s,\lambda} = \frac{1-p_L}{1-\varpi_{0\lambda}p_L}\,\varpi_{0\lambda}i_L, \tag{D1}$$

where p_L is the wavelength independent within-leaf recollision probability, and i_L represents the fraction of radiation scattered at the surface of leaves. The latter is a wavelength-independent function of leaf surface properties. The algorithm results in the following estimate of the DASF (Knyazikhin et al., 2013),

$$\mathrm{DASF}(\Omega;\Omega_0) = \frac{\rho_A(\Omega;\Omega_0)i_0(\Omega_0)}{1-p_A i_L}\,i_L, \tag{D2}$$

where $i_0(\Omega_0)$, $\rho_A(\Omega;\Omega_0)$ and p_A are the canopy interceptance, average escape and recollision probabilities. The retrieved DASF should be normalized by $(1-p_A)i_L/(1-p_A i_L)$ to obtain its LUT counterpart. Site specific values of i_L can be found from measured spectra of leaf albedo (Latorre-Carmona et al., 2014 Schull et al., 2011 Vanhatalo et al., 2014). We followed the methodology documented in Schull et al. (2011).

References

Bonan, G.B., Levis, S., Sitch, S., Vertenstein, M., Oleson, K.W., 2003. A dynamic global vegetation model for use with climate models: concepts and description of simulated vegetation dynamics. Glob. Chang. Biol. 9, 1543–1566.

Bunnik, N.J.J., 1978. The Multispectral Reflectance of Shortwave Radiation by Agricultural Crops in Relation With Their Morphological and Optical Properties.

Chen, J.M., Black, T., 1992. Defining leaf area index for non-flat leaves. Plant Cell Environ. 15, 421–429.

Chen, J.M., Liu, J., Leblanc, S.G., Lacaze, R., Roujean, J.-L., 2003. Multi-angular optical remote sensing for assessing vegetation structure and carbon absorption. Remote Sens. Environ. 84, 516–525.

Chen, J.M., Mo, G., Pisek, J., Liu, J., Deng, F., Ishizawa, M., Chan, D., 2012. Effects of foliage clumping on the estimation of global terrestrial gross primary productivity. Glob. Biogeochem. Cycles 26.

Dai, Y., Dickinson, R.E., Wang, Y.-P., 2004. A two-big-leaf model for canopy temperature, photosynthesis, and stomatal conductance. J. Clim. 17, 2281–2299.

Davis, A.B., Knyazikhin, Y., 2005. A primer in 3D radiative transfer. 3D Radiative Transfer in Cloudy Atmospheres. Springer, pp. 153–242.

Doughty, C.E., Goulden, M.L., 2008. Seasonal patterns of tropical forest leaf area index and CO_2 exchange. J. Geophys. Res. Biogeosci. 2005–2012, 113.

Ganguly, S., Samanta, A., Schull, M.A., Shabanov, N.V., Milesi, C., Nemani, R.R., Knyazikhin, Y., Myneni, R.B., 2008a. Generating vegetation leaf area index Earth system data record from multiple sensors. Part 2: implementation, analysis and validation. Remote Sens. Environ. 112, 4318–4332.

Ganguly, S., Schull, M.A., Samanta, A., Shabanov, N.V., Milesi, C., Nemani, R.R., Knyazikhin, Y., Myneni, R.B., 2008b. Generating vegetation leaf area index earth system data record from multiple sensors. Part 1: theory. Remote Sens. Environ. 112, 4333–4343.

Garrigues, S., Lacaze, R., Baret, F., Morisette, J.T., Weiss, M., Nickeson, J.E., Fernandes, R., Plummer, S., Shabanov, N.V., Myneni, R.B., 2008. Validation and intercomparison of global Leaf Area Index products derived from remote sensing data. J. Geophys. Res. Biogeosci. 113 (G02028), 58–70.

Gerstl, S.A.W., 1999. Building a global hotspot ecology with Triana data. Remote Sens. Earth Sci. Ocean Sea Ice Applic. 3868, 184–194.

Goel, N.S., Qin, W.H., Wang, B.Q., 1997. On the estimation of leaf size and crown geometry for tree canopies from hotspot observations. J. Geophys. Res.-Atmos. 102, 29543–29554.

Goodenough, D.G., Dyk, A., Niemann, K.O., Pearlman, J.S., Hao, C., Tian, H., Murdoch, M., West, C., 2003. Processing hyperion and ALI for forest classification. IEEE Trans. Geosci. Remote Sens. 41, 1321–1331.

He, M., Ju, W., Zhou, Y., Chen, J., He, H., Wang, S., Wang, H., Guan, D., Yan, J., Li, Y., 2013. Development of a two-leaf light use efficiency model for improving the calculation of terrestrial gross primary productivity. Agric. For. Meteorol. 173, 28–39.

Heiskanen, J., Rautiainen, M., Stenberg, P., Mõttus, M., Vesanto, V.-H., Korhonen, L., Majasalmi, T., 2012. Seasonal variation in MODIS LAI for a boreal forest area in Finland. Remote Sens. Environ. 126, 104–115.

Heiskanen, J., Rautiainen, M., Stenberg, P., Mõttus, M., Vesanto, V.-H., 2013. Sensitivity of narrowband vegetation indices to boreal forest LAI, reflectance seasonality and species composition. ISPRS J. Photogramm. Remote Sens. 78, 1–14.

Huang, D., Knyazikhin, Y., Dickinson, R.E., Rautiainen, M., Stenberg, P., Disney, M., Lewis, P., Cescatti, A., Tian, Y., Verhoef, W., 2007. Canopy spectral invariants for remote sensing and model applications. Remote Sens. Environ. 106, 106–122.

Huang, D., Knyazikhin, Y., Wang, W., Deering, D.W., Stenberg, P., Shabanov, N., Tan, B., Myneni, R.B., 2008. Stochastic transport theory for investigating the three-dimensional canopy structure from space measurements. Remote Sens. Environ. 112, 35–50.

Hueni, A., Nieke, J., Schopfer, J., Kneubühler, M., Itten, K.I., 2009. The spectral database SPECCHIO for improved long-term usability and data sharing. Comput. Geosci. 35, 557–565.

Knyazikhin, Y., Marshak, A., 1991. Fundamental equations of radiative transfer in leaf canopies and iterative methods for their solution. In: Myneni, R.B., Ross, J. (Eds.), Photon-Vegetation Interactions: Applications in Plant Physiology and Optical Remote Sensing. Springer-Verlag, Berlin Heidelberg, pp. 9–43.

Knyazikhin, Y., Martonchik, J., Myneni, R., Diner, D., Running, S., 1998a. Synergistic algorithm for estimating vegetation canopy leaf area index and fraction of absorbed photosynthetically active radiation from MODIS and MISR data. J. Geophys. Res. Atmos. 103, 32257–32275 (1984–2012).

Knyazikhin, Y., Martonchik, J.V., Diner, D.J., Myneni, R.B., Verstraete, M., Pinty, B., Gobron, N., 1998b. Estimation of vegetation canopy leaf area index and fraction of absorbed photosynthetically active radiation from atmosphere-corrected MISR data. J. Geophys. Res.-Atmos. 103, 32239–32256.

Knyazikhin, Y., Schull, M.A., Xu, L.A., Myneni, R.B., Samanta, A., 2011. Canopy spectral invariants. Part 1: a new concept in remote sensing of vegetation. J. Quant. Spectrosc. Radiat. Transf. 112, 727–735.

Knyazikhin, Y., Schull, M.A., Stenberg, P., Mottus, M., Rautiainen, M., Yang, Y., Marshak, A., Carmona, P.L., Kaufmann, R.K., Lewis, P., Disney, M.I., Vanderbilt, V., Davis, A.B., Baret, F., Jacquemoud, S., Lyapustin, A., Myneni, R.B., 2013. Hyperspectral remote sensing of foliar nitrogen content. Proc. Natl. Acad. Sci. U. S. A. 110, E185–E192.

Kuusk, A., 1991. The hot spot effect in plant canopy reflectance. Photon-Vegetation Interactions. Springer, pp. 139–159.

Latorre-Carmona, P., Knyazikhin, Y., Alonso, L., Moreno, J.F., Pla, F., Yan, Y., 2014. On hyperspectral remote sensing of leaf biophysical constituents: decoupling vegetation structure and leaf optics using CHRIS–PROBA data over crops in Barrax. IEEE Geosci. Remote Sens. Lett. 11, 1579–1583.

Lewis, P., Disney, M., 2007. Spectral invariants and scattering across multiple scales from within-leaf to canopy. Remote Sens. Environ. 109, 196–206.

Lukeš, P., Stenberg, P., Rautiainen, M., Mõttus, M., Vanhatalo, K.M., 2013. Optical properties of leaves and needles for boreal tree species in Europe. Remote Sens. Lett. 4, 667–676.

Malenovský, Z., Albrechtová, J., Lhotáková, Z., Zurita-Milla, R., Clevers, J.G.P.W., Schaepman, M.E., Cudlín, P., 2006. Applicability of the PROSPECT model for Norway spruce needles. Int. J. Remote Sens. 27, 5315–5340.

Martonchik, J.V., Bruegge, C.J., Strahler, A.H., 2000. A review of reflectance nomenclature used in remote sensing. Remote Sens. Rev. 19, 9–20.

Matthew, M.W., Adler-Golden, S.M., Berk, A., Richtsmeier, S.C., Levine, R.Y., Bernstein, L.S., Acharya, P.K., Anderson, G.P., Felde, G.W., Hoke, M.L., Ratkowski, A.J., Burke, H.-h.K., Kaiser, R.D., Miller, D.P., 2000. Status of Atmospheric Correction Using a MODTRAN4-based Algorithm. pp. 199–207.

Mercado, L.M., Bellouin, N., Sitch, S., Boucher, O., Huntingford, C., Wild, M., Cox, P.M., 2009. Impact of changes in diffuse radiation on the global land carbon sink. Nature 458, 1014–1017.

Miller, J., 1967. A formula for average foliage density. Aust. J. Bot. 15, 141–144.

Nilson, T., 1991. Approximate analytical methods for calculating the reflection functions of leaf canopies in remote sensing applications. Photon-Vegetation Interactions. Springer, pp. 161–190.

Norman, J.M., 1982. Simulation of microclimates. Biometeorology in Integrated Pest Management, pp. 65–99.
Otsu, N., 1975. A threshold selection method from gray-level histograms. Automatica 11, 23–27.
Pearlman, J.S., Barry, P.S., Segal, C.C., Shepanski, J., Beiso, D., Carman, S.L., 2003. Hyperion, a space-based imaging spectrometer. IEEE Trans. Geosci. Remote Sens. 41, 1160–1173.
Qin, W., Goel, N.S., Wang, B., 1996. The hotspot effect in heterogeneous vegetation canopies and performances of various hotspot models. Remote Sens. Rev. 14, 283–332.
Qin, W.H., Gerstl, S.A.W., Deering, D.W., Goel, N.S., 2002. Characterizing leaf geometry for grass and crop canopies from hotspot observations: a simulation study. Remote Sens. Environ. 80, 100–113.
Rautiainen, M., Lukeš, P., 2015. Spectral contribution of understory to forest reflectance in a boreal site: an analysis of EO-1 Hyperion data. Remote Sens. Environ. 171, 98–104.
Rautiainen, M., Stenberg, P., 2015. On the angular dependency of canopy gap fractions in pine, spruce and birch stands. Agric. For. Meteorol. 206, 1–3.
Rautiainen, M., Mõttus, M., Stenberg, P., Ervasti, S., 2008. Crown envelope shape measurements and models. Silva Fenn. 42, 19–23.
Rautiainen, M., Mõttus, M., Stenberg, P., 2009. On the relationship of canopy LAI and photon recollision probability in boreal forests. Remote Sens. Environ. 113, 458–461.
Rautiainen, M., Mõttus, M., Heiskanen, J., Akujärvi, A., Majasalmi, T., Stenberg, P., 2011. Seasonal reflectance dynamics of common understory types in a northern European boreal forest. Remote Sens. Environ. 115, 3020–3028.
Ross, J., 1981. The Radiation Regime and Architecture of Plant Stands. Dr W. Junk Publishers.
Ross, J.K., Marshak, A.L., 1988. Calculation of canopy bidirectional reflectance using the Monte-Carlo method. Remote Sens. Environ. 24, 213–225.
Schaepman-Strub, G., Schaepman, M.E., Painter, T.H., Dangel, S., Martonchik, J.V., 2006. Reflectance quantities in optical remote sensing-definitions and case studies. Remote Sens. Environ. 103, 27–42.
Schull, M.A., Knyazikhin, Y., Xu, L., Samanta, A., Carmona, P.L., Lepine, L., Jenkins, J.P., Ganguly, S., Myneni, R.B., 2011. Canopy spectral invariants, part 2: application to classification of forest types from hyperspectral data. J. Quant. Spectrosc. Radiat. Transf. 112, 736–750.
Smolander, S., Stenberg, P., 2003. A method to account for shoot scale clumping in coniferous canopy reflectance models. Remote Sens. Environ. 88, 363–373.
Smolander, S., Stenberg, P., 2005. Simple parameterizations of the radiation budget of uniform broadleaved and coniferous canopies. Remote Sens. Environ. 94, 355–363.
Stenberg, P., 1998. Implications of shoot structure on the rate of photosynthesis at different levels in a coniferous canopy using a model incorporating grouping and penumbra. Funct. Ecol. 12, 82–91.
Stenberg, P., 2006. A note on the G-function for needle leaf canopies. Agric. For. Meteorol. 136, 76–79.
Stenberg, P., 2007. Simple analytical formula for calculating average photon recollision probability in vegetation canopies. Remote Sens. Environ. 109, 221–224.
Stenberg, P., Mõttus, M., Rautiainen, M., 2016. Photon recollision probability in modelling the radiation regime of canopies — a review. Remote Sens. Environ. 183, 98–108.
Stoyan, D., Kendall, S.W., Mecke, J., 1995. Stochastic Geometry and Its Applications. John Wiley & Sons, New York.
Sun, L., Neville, R., Staenz, K., White, H.P., 2008. Automatic destriping of hyperion imagery based on spectral moment matching. Can. J. Remote. Sens. 34, S68–S81.
Vainikko, G.M., 1973. Transfer approach to the mean intensity of radiation in non-continuous clouds. Trudy MGK SSSR. Meteorol. Invest. 21, 28–37.
Vanhatalo, K.M., Rautiainen, M., Stenberg, P., 2014. Monitoring the broadleaf fraction and canopy cover of boreal forests using spectral invariants. J. Quant. Spectrosc. Radiat. Transf. 133, 482–488.
Vladimirov, V., 1963. Mathematical Problems in the One-Velocity Theory of Particle Transport. Atomic Energy of Canada Limited Chalk River, Ontario.
Wang, S., Grant, R., Verseghy, D., Black, T., 2001. Modelling plant carbon and nitrogen dynamics of a boreal aspen forest in CLASS—the Canadian Land Surface Scheme. Ecol. Model. 142, 135–154.
Wang, Y.J., Buermann, W., Stenberg, P., Smolander, H., Hame, T., Tian, Y.H., Hu, J.N., Knyazikhin, Y., Myneni, R.B., 2003. A new parameterization of canopy spectral response to incident solar radiation: case study with hyperspectral data from pine dominant forest. Remote Sens. Environ. 85, 304–315.
Wilson, J.W., 1967. Stand structure and light penetration. III. Sunlit foliage area. J. Appl. Ecol. 4, 159–165.
Yan, K., Park, T., Yan, G., Chen, C., Yang, B., Liu, Z., Nemani, R., Knyazikhin, Y., Myneni, R., 2016a. Evaluation of MODIS LAI/FPAR product collection 6. Part 1: consistency and Improvements. Remote Sens. 8, 359.
Yan, K., Park, T., Yan, G., Liu, Z., Yang, B., Chen, C., Nemani, R., Knyazikhin, Y., Myneni, R., 2016b. Evaluation of MODIS LAI/FPAR product collection 6. Part 2: validation and intercomparison. Remote Sens. 8, 460.
Yang, B., Knyazikhin, Y., Lin, Y., Yan, K., Chen, C., Park, T., Choi, S., Mõttus, M., Rautiainen, M., Myneni, R., Yan, L., 2016. Analyses of impact of needle surface properties on estimation of needle absorption spectrum: case study with coniferous needle and shoot samples. Remote Sens. 8, 563.